

# Spectroscopic Binaries in Globular Clusters. II. A Search for Long-Period Binaries in M22

Patrick Côté<sup>1,2</sup>

Dominion Astrophysical Observatory, Herzberg Institute of Astrophysics, National Research Council of  
Canada, 5071 W. Saanich Road, R.R.5, Victoria, BC, V8X 4M6, Canada  
cote@dao.nrc.ca

Carlton Pryor<sup>3</sup>

Department of Physics and Astronomy, Rutgers, The State University, Box 0849  
Piscataway, New Jersey 08855-0849, USA  
pryor@physics.rutgers.edu

and

Robert D. McClure<sup>3</sup>, J. M. Fletcher<sup>3</sup>, James E. Hesser<sup>3</sup>

Dominion Astrophysical Observatory, Herzberg Institute of Astrophysics, National Research Council of  
Canada, 5071 W. Saanich Road, R.R.5, Victoria, BC, V8X 4M6, Canada  
mcclure@dao.nrc.ca, fletcher@dao.nrc.ca, hesser@dao.nrc.ca

Received \_\_\_\_\_; accepted \_\_\_\_\_

To appear in the Astronomical Journal

---

<sup>1</sup>Visiting Astronomer, Cerro Tololo Inter-American Observatory. CTIO is operated by AURA, Inc. under contract to the National Science Foundation.

<sup>2</sup>Visiting Astronomer, Kitt Peak National Observatory. KPNO is operated by AURA, Inc. under contract to the National Science Foundation.

<sup>3</sup>Visiting Astronomer, Canada-France-Hawaii Telescope operated by the National Research Council of Canada, the Centre National de la Recherche Scientifique de France and the University of Hawaii.

## ABSTRACT

A catalog of 383 radial velocities (median accuracy  $\simeq 1 \text{ km s}^{-1}$ ) for red giants in the Galactic globular cluster M22 has been compiled from the literature and from new observations accumulated between 1972 and 1994. This 22-year baseline is the longest available for any sample of globular cluster stars. Using 333 repeat velocities for 109 cluster members, we have carried out a search for spectroscopic binaries with periods in the range  $0.2 \lesssim P \leq 40$  years and with mass ratios between 0.1 and 1.0. Although the radial velocities for these evolved stars show clear evidence for an atmospheric “jitter” whose magnitude depends on luminosity, no star is convincingly found to exhibit a velocity variation greater than  $7 \text{ km s}^{-1}$ . By comparing the observed velocity variations to those found in a series of Monte-Carlo simulations, we estimate the cluster binary fraction to be  $x_b = 0.01_{-0.01}^{+0.10}$  (circular orbits) and  $x_b = 0.03_{-0.03}^{+0.16}$  (thermal orbits), where the uncertainties are 90% confidence limits. These results are to be compared to the corresponding binary fraction of  $x_b = 0.12 \pm 0.03$  for nearby, solar-type stars having similar mass ratios and periods. We speculate that both the relative abundances of short- and long-period binaries in globular clusters and the large differences in measured binary fractions for clusters with high binary ionization rates (M22,  $\omega$  Cen) compared to those clusters with low ionization rates (M71, M4, NGC 3201) point to a frequency-period distribution in which “soft” binaries have been disrupted by stellar encounters. Finally, we note that none of the three CH stars in our survey shows evidence for velocity variations; this is in stark contrast to *field* CH stars, virtually all of which are binaries. We argue that binaries in M22 which have binding energies similar to field CH stars are unlikely to have been disrupted and suggest that the cluster CH stars are otherwise normal red giants which lie in the carbon-enriched tail of the cluster metallicity distribution function.

*Subject headings:* globular clusters: individual (M22) — stars: binaries — stars: carbon — techniques: radial velocities

## 1. Introduction

The binary fraction,  $x_b$ , is a fundamental parameter of any stellar population. For dense stellar systems like globular clusters, it is also an essential ingredient for realistic models of their dynamical evolution. The first efforts to measure  $x_b$  for globular clusters led to the surprising conclusion that they were markedly deficient in binaries relative to the field (e.g., Gunn & Griffin 1979). This result became difficult to understand in the light of numerical simulations (e.g., Cohn 1980) which demonstrated repeatedly that, in the absence of an additional heat source such as that provided by a population of primordial binaries, most Galactic globular clusters should by now have settled into a state of core collapse. Early ground-based surveys, however, indicated that, at most, only  $\sim 20\%$  of Galactic globular clusters exhibit the telltale central brightness cusp predicted by core-collapse models (Djorgovski & King 1986). The large numbers of blue stragglers seen in many globulars is additional indirect evidence for the existence of cluster binaries. Although it remains to be seen whether the bulk of these cluster blue stragglers formed via stellar collisions (e.g., Hoffer 1983) or through coalescence of close pairs (Zinn & Searle 1976), it now appears likely that binaries play a key role in their formation.

A number of recent observational studies have concluded that the globular cluster binary fraction is roughly comparable to that of the Population I field (e.g., Hut et al. 1992; Côté et al. 1994; Yan & Mateo 1994). Nevertheless, our knowledge of the *shape* of the distribution of binary star periods in globular clusters remains remarkably limited. For instance, the distribution of orbital periods among nearby, solar-type stars is closely Gaussian in  $\log P$  with a peak near 180 yr and a dispersion  $\sigma_{\log P} \simeq 2.3$  (Duquennoy & Mayor 1991). Does the globular cluster period distribution differ significantly from this field distribution? There are strong reasons to believe that it *must*, since stellar encounters will tend to disrupt “soft” binaries and harden already “hard” systems (Heggie 1975). Hills (1984) found that the semi-major axis of the widest binary which is expected to have escaped disruption by encounters with single stars is

$$a_c = 12.4 \text{ AU} \left( \frac{M_1 + M_2}{1.4 M_\odot} \right) \left( \frac{10 \text{ km s}^{-1}}{\sigma} \right)^2, \quad (1)$$

where  $\sigma$  is the three-dimensional rms cluster velocity dispersion in  $\text{km s}^{-1}$  and  $M_1$  and  $M_2$  are the primary and secondary masses in solar units. Binaries with separations greater than  $a_c$  are expected to be disrupted in a Hubble time, provided  $\sigma$  and the cluster number density of stars,  $n$ , satisfy (Pryor et al. 1996)

$$\left( \frac{n}{1 \text{ pc}^{-3}} \right) \left( \frac{5 \text{ km s}^{-1}}{\sigma} \right)^3 > 106. \quad (2)$$

This relation, which is based on the ionization rate of Hut & Bahcall (1983) and assumes  $0.8M_{\odot}$  stars, is satisfied at the centers of most clusters. According to Pryor & Meylan (1993), Galactic globular clusters have  $2 \lesssim \sigma \lesssim 25 \text{ km s}^{-1}$  with a mean near  $\simeq 8 \text{ km s}^{-1}$ . Consequently, the widest surviving systems will have  $3 \lesssim P_c \lesssim 5000$  years, with a typical upper period cutoff of  $P_c \simeq 80$  years (assuming  $M_1$  and  $M_2 = 0.8M_{\odot}$ ). Dynamical processes are therefore likely to have played an important role in modifying the initial distribution of orbital periods in globular clusters.

Unfortunately, existing data are not well suited to the task of detecting long-period binaries. For instance, studies of binaries based on the so-called “second sequence” in the cluster color-magnitude diagram are *period degenerate* (i.e., equally sensitive to binaries of *all* periods). On the other hand, searches for eclipsing binaries (e.g., Mateo 1996) are sensitive only to systems with periods near one day and are virtually blind to binaries with periods in excess of  $\sim 10$  days (Mateo 1993). Although the situation is greatly improved for radial velocity surveys, studies to date have been limited to binaries containing red giants with periods longer than 1–2 months and shorter than 5–20 years. The lower limit is set by selection effects caused by possible mass transfer between the binary components (see Pryor, Latham & Hazen 1988), whereas the upper cutoff is simply a consequence of the limited duration (and velocity accuracy) of existing radial velocity surveys. In this paper, we combine previously published radial velocities for red giants in the nearby cluster M22 with new measurements accumulated between 1972 and 1994 to search for spectroscopic binaries with periods in the range 0.2 to 40 years, a factor of two improvement over existing surveys in the upper period cutoff. In a companion paper (Côté & Fischer 1996), we report on an investigation of the *short-period* end of the globular cluster binary distribution (i.e.,  $2 \text{ day} \lesssim P \lesssim 3 \text{ years}$ ) based on radial velocities for stars on the upper main-sequence of the nearby cluster M4.

## 2. Observations

### 2.1. Photometry

As described in §3, our technique of determining  $x_b$  from a series of Monte-Carlo simulations requires an estimate of the radius of each star in order to assess the likelihood of Roche-lobe overflow on an object-by-object basis. Such radii are most easily obtained by comparing the location of each star in the cluster color-magnitude diagram (CMD) with the appropriate isochrone (see Côté et al. 1994 for details).

However, six of the red giants in our survey have no published magnitudes or colors since they are located either at large distance from the cluster center or in the crowded core of the cluster — areas which were specifically avoided in previous photometric studies. Moreover, the available photometry for the remaining objects (almost all of which is photographic in nature) must be assembled from a number of different sources (e.g. Peterson & Cudworth 1994; Lloyd Evans 1975; Arp & Melbourne 1959).

In order to obtain a homogeneous set of magnitudes and colors for *all* stars in our survey, we used the KPNO 0.9m telescope on 1995 July 8/9 with the T2KA 2048×2048 CCD (scale =  $0''.68 \text{ pixel}^{-1}$ , gain =  $10.7 \text{ e}^- \text{ ADU}^{-1}$ , readnoise =  $4 \text{ e}^-$ ) to image five overlapping fields in the direction of M22. We obtained a BV frame pair centered on M22 and four other fields offset by  $14'.3$  in the NW, NE, SW and SE directions, giving a total field of view of 0.52 square degrees. Seeing during the exposures was typically  $\simeq 1''.8$ . A finding chart for the six stars without previous photometry is given in Figure 1. After standard preprocessing with IRAF,<sup>4</sup> a CMD for the entire field was derived using DAOPHOT II (Stetson, Davis & Crabtree 1990) and the related software package ALLFRAME (Stetson 1994). Unfortunately, observing conditions were nonphotometric, making a direct calibration of the photometry impossible. We instead used 22 isolated, local photoelectric standards from Alcaïno, Liller & Alvarado (1988) to calibrate the data. Figure 2 shows a comparison between our CCD photometry and the photographic data of Peterson & Cudworth (1994) for the 137 radial velocity members which are common to both studies (see §2.2). There is a tendency for our V magnitudes to be 0.05 mag fainter than those of Peterson & Cudworth (1994). We also find a similar offset in color,  $\Delta(B-V) = 0.06 \text{ mag}$ , in the sense that our derived colors are bluer than the photographic values. The sense of the  $\Delta V$  offset from the Peterson & Cudworth (1994) photometry is the same as that reported in the recent CCD study of the cluster core by Anthony-Twarog, Twarog & Craig (1995), although not quite as large: 0.05 mag compared to 0.09 mag. Unfortunately, since Anthony-Twarog, Twarog & Craig (1995) did not obtain B photometry for their program stars, a direct comparison of the CCD colors is impossible.

The CMD for the entire  $43'.2 \times 43'.2$  field is shown in the upper panel of Figure 3. As expected, the field star contamination near M22 ( $l = 9^\circ.9$ ,  $b = -7^\circ.6$ ) is severe. The lower panel of Figure 3 shows those stars within five core radii ( $r_c = 1'.42$  according to Trager, King & Djorgovski 1995) of the Shawl & White (1986)

---

<sup>4</sup>IRAF is distributed by the National Optical Astronomy Observatories, which are operated by the Association of Universities for Research in Astronomy, Inc., under contract to the National Science Foundation.

cluster center. The large open squares indicate the three known photometric variables in our sample, for which we have adopted the mean magnitudes and colors reported by Peterson & Cudworth (1994). The small squares indicate the remaining 106 cluster red giants with multiple velocity measurements.

## 2.2. Spectroscopy

An observing log of all spectroscopic observations used in our survey is given in Table 1, whose columns record, from left to right, the date of the observing run, the telescope and accompanying instrumentation, the number of separate velocity measurements, and the total number of stars which were observed. We now discuss each of these data sets in turn.

As one of the nearest globular clusters (e.g., Djorgovski 1993 quotes a distance of 3 kpc), M22 was an early target for high resolution spectroscopy of individual cluster giants. In their landmark dynamical study of M3, Gunn & Griffin (1979) allude to the existence of several dozen, unpublished radial velocities for stars in a number of other clusters, including M22, which were collected with the Hale 5m telescope and Palomar radial velocity scanner during the 1970s. The entire sample of Hale radial velocities for M22 giants (67 observations of 44 different stars), accumulated during a series of observing runs in 1972, 1974 and 1975, were kindly donated by Drs. Griffin and Gunn. For a complete description of the design and operation of the Palomar radial velocity scanner, the reader is referred to Griffin & Gunn (1974) and Gunn & Griffin (1979).

In addition to these data, a total of 176 radial velocities for 130 red giants in M22 have recently been published by Peterson & Cudworth (1994). These velocities, accumulated during the 1985 – 1987 observing seasons with the SAO 1.5m and MMT telescopes, have a precision similar to the Hale observations (e.g., typical uncertainty  $\simeq 1 \text{ km s}^{-1}$ ). For a detailed description of the SAO observations and reductions, the reader is referred to Peterson & Cudworth (1994). We obtained a third set of velocities using the DAO radial velocity scanner (Fletcher et al. 1982) on the CFHT during a pair of observing runs in 1989 and 1991. A total of 49 radial velocities for 36 stars (chosen from the finder charts of Lloyd Evans 1975 and Cudworth 1986) were measured over three nights. The velocity accuracy delivered by this combination of telescope and instrument is also  $\simeq 1 \text{ km s}^{-1}$ . A complete description of this instrument’s operation at the coudé focus of the CFHT may be found in Pryor et al. (1989). Our final epoch consists of radial velocities (median precision  $\simeq 1.6 \text{ km s}^{-1}$ ) for 92 giants obtained with the CTIO 4m telescope and the

Argus multi-object spectrograph in June 1994. Targets were selected from the list of confirmed cluster members given in Peterson & Cudworth (1994). The primary goal of this observing run was to measure velocities for turnoff dwarfs in the nearby globular cluster M4, the results of which are presented by Côté & Fischer (1996). Since the reduction procedures followed in the M22 analysis are identical to those used in our study of M4, the reader is referred to that paper for details.

To ensure that all of these radial velocities share a common zeropoint, we have applied small offsets to the Hale, CFHT and CTIO observations. These corrections, which never exceeded  $1 \text{ km s}^{-1}$ , were determined by matching all stars in common with the SAO/MMT catalog (which is the most extensive data set and has the most closely monitored zeropoint). The entire sample of M22 radial velocities is given in Table 2 (also presented in the ApJ/AJ CD-ROM Series, Volume X, 1996). Since these data may be useful for other purposes, we have tabulated *all* known radial velocity members of M22; that is to say, cluster members with only a single radial velocity measurement are included. Table 2 therefore consists of 383 radial velocities for 162 different stars. Of these, 109 objects have more than one measurement. Excluding the three known photometric variables in this sample (i.e., stars V5, V8, and V9; Sawyer-Hogg 1973), we find a systemic velocity of  $-148.55 \pm 0.56 \text{ km s}^{-1}$  and a one dimensional velocity dispersion of  $7.06 \pm 0.40 \text{ km s}^{-1}$  using the maximum-likelihood method of Pryor & Meylan (1993). From left to right, Table 2 gives the star number, the ID from Peterson & Cudworth (1994), the distance in arcminutes from the Shawl & White (1986) cluster center, the position angle in degrees, the heliocentric Julian date, the radial velocity, the weighted mean velocity, the reduced chi-squared and the probability  $P(\chi^2)$  of that chi-squared value being exceeded assuming that the velocity is constant, the V magnitude and B–V color measured from our CCD frames, and the source of the radial velocity (P = Palomar, S = SAO, C = CFHT, and T = CTIO).

Most previous surveys of red giants in globular clusters have found evidence for a velocity “jitter” which is assumed to arise from convective or pulsational motions in the atmospheres of these evolved stars (Gunn & Griffin 1979; Mayor et al. 1984; Lupton, Gunn & Griffin 1987; Pryor, Latham & Hazen 1988). Gunn & Griffin (1979) found it necessary to included an external dispersion of  $0.8 \text{ km s}^{-1}$  to account for the low-amplitude velocity variations observed in their sample of M3 giants. Using an expanded sample of M3 velocities, Pryor, Latham & Hazen (1988) concluded that, while the velocity variability was probably present in the entire sample of program objects, it was certainly largest for those stars within 0.5 magnitude of the giant-branch tip. We too find evidence for such a luminosity-dependent velocity jitter in our sample of M22 giants. Figure 4 shows the dependence of  $P(\chi^2)$  on V magnitude and B–V color for the 106 stars with multiple velocity measurements (photometric variables excluded). No jitter has been assumed in

deriving the probabilities shown in Figure 4. Four stars with  $P(\chi^2) \leq 0.001$  are indicated by the vertical arrows. As Figure 4 demonstrates, there is a tendency for stars near the tip of the giant branch to have the lowest probabilities. This effect can also be seen by dividing our sample into three broad luminosity bins: a bright sample of 13 stars ( $V \leq 11.5$ ), an intermediate sample of 32 stars ( $11.5 \leq V \leq 12.4$ ) and a faint sample ( $12.4 \leq V \leq 13.65$ ) of 61 stars. The respective number of objects with  $P(\chi^2) \leq 0.5$  in each of these three bins are 11 (85%), 22 (69%), and 30 (49%), which demonstrates that the size of the jitter is indeed luminosity-dependent.

After some experimentation, we adopted a velocity jitter which is constant for those stars within  $\simeq 0.5$  magnitude of the tip of the RGB and which linearly decreases to zero below this level:

$$\begin{aligned} \sigma_j &= 0.9 \text{ km s}^{-1} && \text{if } V \leq 11.55 \\ \sigma_j &= (0.9/2.45)(14.0 - V) \text{ km s}^{-1} && \text{if } 11.55 < V \leq 14.00 \\ \sigma_j &= 0 \text{ km s}^{-1} && \text{if } V > 14.00 \end{aligned} \tag{3}$$

Adding this jitter in quadrature to the formal velocity uncertainties given in Table 2 lowers the number of stars with  $P(\chi^2) \leq 0.5$  in each of the three luminosity bins to 8 (62%), 13 (41%), and 30 (49%), respectively. The resulting histogram of  $P(\chi^2)$  is given in the upper panel of Figure 5. For a sample of constant-velocity stars, such a distribution should be nearly flat (provided, of course, that the velocity uncertainties are correctly estimated). A population of stars with variable velocities will manifest itself as a peak near zero probability. Apart from a modest enhancement near  $P(\chi^2) \approx 0.00$ , the histogram is clearly consistent with a flat distribution (indicated by the dashed line).

The heavy line in the lower panel of Figure 5 shows the cumulative distribution of  $P(\chi^2)$ . The distribution expected for a sample of constant-velocity stars is indicated by the dashed diagonal line. This technique avoids the problem of binning the data which is inherent in the above approach (although it should be kept in mind that the individual points are no longer statistically independent). The good agreement between the two distributions lends credence to our adopted jitter and suggests that it is unlikely that our M22 sample contains an appreciable number of bona fide radial velocity variables. As a further demonstration of the validity of our adopted velocity jitter, we show the probability distributions for the two cases of: (1) no velocity jitter (upper line); and (2) a jitter of  $1.5 \text{ km s}^{-1}$  which is independent of luminosity (lower line). These distributions bracket that obtained using equation 3 and provide a much poorer match to the distribution expected for a sample composed primarily of constant-velocity stars. Regardless of the precise size and luminosity dependence of the external dispersion, our estimate for the



cluster binary fraction is based solely on the number of stars showing velocity variations greater than 8 km s<sup>-1</sup>. As a result, our best-fit binary fraction is essentially independent of the adopted jitter (see §4).

### 3. Monte-Carlo Simulations

Extracting a binary fraction from a catalog of radial velocities is a formidable task, since the number of stars expected to show large radial velocity variations depends on the number, spacing, and precision of the observed radial velocities, as well as the distribution of orbital periods, mass ratios, eccentricities, inclinations, and the longitudes and times of periastron passage. Since an *a priori* knowledge of the form of these distributions is, of course, unavailable, the best approach is to generate simulated radial velocity catalogs with known binary fractions. By comparing the simulated observations to the actual data, it is possible to determine both  $x_b$  and its associated confidence range. The Monte-Carlo approach used here is similar to that employed in several earlier studies (Hut et al. 1992; Côté et al. 1994), to which the reader is referred for more details.

First, we compute a radius for each star based on its location in the CMD using the 14 Gyr, [Fe/H] = -1.78 isochrone of Bergbusch & Vandenberg (1992). (We adopt a distance of 3 kpc and a metallicity of [Fe/H] = -1.75; Djorgovski 1993.) Figure 6 shows the Bergbusch & Vandenberg (1992) radius-magnitude relation used to compute the radii  $R$  of our stars. Second, for each simulation, we *assume* a binary fraction and randomly assign binary or single star status to each program object using  $x_b$  as the probability of selecting a binary. For single stars, we generate the same number of radial velocities as in the actual catalog and include a realistic amount of observational noise (i.e.,  $\sigma^2 = \sigma_f^2 + \sigma_j^2$  where  $\sigma_f$  is the formal uncertainty recorded in Table 2 and  $\sigma_j$  is the external dispersion given by equation 3). For binary stars, we randomly assign an orbital period  $P$  and mass ratio,  $q = M_2/M_1$ . We adopt distributions for  $P$  and  $q$  which are based on those found by Duquennoy & Mayor (1991) in their study of multiplicity among nearby, solar-type stars. Specifically, we adopt a period distribution of the form

$$\frac{dN}{d\log P} \propto \exp\left(-\frac{(\log P - \overline{\log P})^2}{2\sigma_{\log P}^2}\right), \quad (4)$$

where  $P$  is in days,  $\overline{\log P} = 4.8$  and  $\sigma_{\log P} = 2.3$ . For the distribution of mass ratios, we adopt the Duquennoy & Mayor (1991) relation

$$\frac{dN}{dq} \propto \exp\left(-\frac{(q - \overline{q})^2}{2\sigma_q^2}\right), \quad (5)$$

where  $\bar{q} = 0.23$  and  $\sigma_q = 0.42$ . Our adopted upper and lower cutoffs for these distributions are discussed below.

Simulations are carried out for two assumed eccentricity distributions: (1) purely circular orbits,  $e = 0$ ; and (2) a thermal distribution of eccentricities,  $f(e) = 2e$  (Heggie 1975). The final step is to assign random values to each of the remaining orbital parameters and test for the possibility of mass transfer between the components using the prescription given in Pryor, Latham & Hazen (1988). If the binary is found to be sufficiently compact that Roche-Lobe overflow is likely, we assume that the system has been removed from the sample (see Pryor, Latham & Hazen 1988) and repeat the entire procedure. If mass transfer has *not* occurred, we generate the appropriate number of radial velocities for each star, including, as before, a realistic amount of observational noise. For a grid of  $x_b$  running from 0.00, 0.01, 0.02,..., 0.60 we generate 1000 simulated catalogs and calculate the mode of the number of stars which show velocity variations greater than  $8 \text{ km s}^{-1}$ , a value chosen to avoid possible complications caused by measurement error and/or atmospheric motions (which can sometimes approach  $8 \text{ km s}^{-1}$  for long-period variables near the tip of the giant branch; Hut et al. 1992).

Needless to say, a crucial first step in the analysis is to determine the range of orbital periods and mass ratios to which our observations are sensitive. We measure our *binary discovery efficiency* by determining the fraction of known binary stars in each simulation which are recovered as binaries by exhibiting velocity variations greater than  $8 \text{ km s}^{-1}$ . Figure 7 shows our binary discovery efficiencies as a function of orbital period for the two cases of circular and thermal orbits. To illustrate the effects of mass transfer between the components, we display the discovery efficiencies before (solid curves) and after (dashed curves) taking mass transfer into account. We conclude that our survey should be sensitive to binaries with  $0.1 \leq q \leq 1.0$  and  $0.2 \lesssim P \leq 40$  years, where the approximate lower limit on  $P$  reflects the fact that the actual cutoff used in the simulations was 0.1 years for circular orbits and 0.3 years for thermal orbits.

## 4. Results

Only one of our program stars (V-23) shows a velocity variation larger than  $8 \text{ km s}^{-1}$ . The reality of this variation, however, is questionable since four of the five velocities for this star (which span nearly 20 years) are in good agreement at  $v_r \simeq -138.5 \text{ km s}^{-1}$ . The remaining velocity — that obtained in July 1989 with the CFHT — is in disagreement by more than  $12 \text{ km s}^{-1}$  (i.e.,  $v_r = -150.76 \text{ km s}^{-1}$ ). Moreover, V-23

is located in the crowded core of the cluster and just  $10''$  from the star I-202 which has  $v_r = -151.85 \text{ km s}^{-1}$  based on a single measurement with the Hale 5m telescope. We therefore suspect that V-23 may have been misidentified during the July 1989 CFHT run, although continued monitoring of this star is clearly in order since, at present, we cannot rule out the possibility that it is an eccentric binary. In what follows, we give the binary fractions which result if we: (1) *discard* the July 1989 measurement (Case A); and (2) *retain* the July 1989 measurement (Case B). For Case A, the observed velocity variation of V-23 drops to  $2.00 \text{ km s}^{-1}$ . The stars with the largest velocity variations in the Case A sample are then III-35 and IV-97 which shows changes in radial velocity of  $6.92 \text{ km s}^{-1}$  and  $6.90 \text{ km s}^{-1}$ , respectively.

For each simulated dataset, we count the number of stars,  $N_8$ , which show a velocity variation greater than  $8 \text{ km s}^{-1}$ . The procedure is repeated 1000 times for each  $x_b$  and we take the mode of the resulting distribution as the value of  $N_8$  appropriate for the adopted binary fraction. We then determine the cluster binary fraction by finding the  $x_b$  for which the *observed* and *simulated* values of  $N_8$  are equal. To get the 90% confidence limits on the derived binary fraction, we find: (1) the *smallest* value of  $x_b$  which produces a value of  $N_8$  which equals or exceeds the actual value less than 5% of the time and; (2) the *largest* value of  $x_b$  which gives a value of  $N_8$  which is equal to or less than the actual value less than 5% of the time. For Case A, we find acceptable matches (i.e.,  $N_8 = 0$ ) between the simulated and actual data for binary fractions in the range  $0.00 \leq x_b \leq 0.01$  (circular orbits) and  $0.00 \leq x_b \leq 0.03$  (thermal orbits). The 90% confidence intervals for these estimates are  $0.00 \leq x_b \leq 0.11$  and  $0.00 \leq x_b \leq 0.19$ , respectively. The binary fractions for Case B (i.e.,  $N_8 = 1$ ) are  $0.02 \leq x_b \leq 0.05$  (circular orbits) and  $0.04 \leq x_b \leq 0.12$  (thermal orbits), with respective 90% confidence intervals of  $0.00 \leq x_b \leq 0.18$  and  $0.00 \leq x_b \leq 0.29$ . These values of  $x_b$  refer to the fraction of primaries on the main sequence with  $0.2 \lesssim P \leq 40$  years and  $0.1 \leq q \leq 1.0$ .

How sensitive are these estimates to our adopted model parameters? To answer this question we have derived  $x_b$  and its corresponding 90% confidence limits using a number of different model assumptions. The results of these experiments are summarized in Table 3. Specifically, we have investigated the effect of: (1) increasing the lower cutoff of the secondary mass distribution (model b); (2) increasing the upper cutoff in the secondary mass distribution (equivalent to including some massive degenerate secondaries) (model c); (3) selecting periods and mass ratios from logarithmically *flat* distributions (model d); (4) disregarding the presence of velocity jitter (model e); (5) decreasing the upper period cutoff by a factor of two (model f); and (6) selecting only equal-mass components (model g). In general, the changes in the derived binary fractions produced by these various assumptions are small compared to the 90% confidence intervals on  $x_b$ . The sole exception is model g, which assumes equal mass components. In this case, the upper limits

on the derived binary fraction drop by nearly a factor of two since binaries with equal mass components show relatively large velocity variations and are, therefore, easier to detect. In short, the two factors which limit the precision of existing measurements of  $x_b$  based on the velocities of red giants remain the unknown distribution of orbital eccentricities and the statistical uncertainties due to small samples of stars. Considerable progress toward overcoming the second of these difficulties is expected in the next few years, as repeat velocities for hundreds, or in some cases, thousands of globular cluster stars are accumulated with multi-object spectrographs (e.g., Gebhardt et al. 1995).

We now compare our best-fit (i.e., Case A) binary fractions of  $x_b = 0.01^{+0.10}_{-0.01}$  (circular orbits) and  $x_b = 0.03^{+0.16}_{-0.03}$  (thermal orbits) to that found among nearby field stars. The most comprehensive study of multiplicity among Population I field stars is that of Duquennoy & Mayor (1991), who surveyed 164 primaries in the spectral range F7 to G9. Their complete sample contains 21 binaries with periods between 0.1 and 40 years (our detection limits for circular orbits) and 20 systems with periods in the range 0.3 to 40 years (our limits for thermal orbits). If we add one star to account for incompleteness and multiply by 0.88 to remove binaries having mass ratios less than 0.1, we find  $x_b \simeq 0.12 \pm 0.03$ . This is the Population I binary fraction to be compared to that of M22. This is considerably larger than that found for M22, though we caution that the 90% confidence intervals on the derived binary fraction still overlap the Population I estimate.

Binary fractions based on radial velocity surveys have now been published for several other globular clusters, the results of which are summarized in Table 4a. The first four columns of this table record the name of the cluster(s), the binary fraction for systems with mass ratios in the range  $0.1 \leq q \leq 1.0$ , the shortest and longest periods detectable in the survey ( $P_{\min}$  and  $P_{\max}$ , respectively), and  $x_b/\log(P_{\max}/P_{\min})$ , the measured binary fraction per decade of period (which has the advantage that it removes, to some extent, the dependence of  $x_b$  on the adopted period range). We begin the discussion of these cluster binary fractions by comparing them to the value reported by Yan & Mateo (1994) based on the five eclipsing binaries that they found in M71:  $x_b = 0.013$  for systems with periods in the range 2.5 to 5 days. Using their binary fraction to extrapolate to the period interval sampled by the radial velocity surveys reviewed by Hut et al. (1992), these authors concluded that “existing data on short-period and red-giant binaries favor a flat frequency-period distribution over the distribution given in Duquennoy & Mayor (1991).” However, with a one-dimensional velocity dispersion of  $\sigma_{1D} \simeq 2.2 \text{ km s}^{-1}$ , M71 represents a dynamical environment which is quite different from the bulk of the clusters in the Hut et al. (1992) sample (which have  $\overline{\sigma}_{1D} \simeq 6.3 \text{ km s}^{-1}$ ; see below). Ideally, one would like to compare the abundances of short- and long-period binaries

in the *same* cluster or, at least, in clusters having similar velocity dispersions and stellar densities. It is also worth bearing in mind that both the Yan & Mateo (1994) and Hut et al. (1992) binary fractions are uncertain by roughly a factor of two: the former as a result of the poorly known coalescence timescales of contact binaries and the latter as a result of the low binary discovery efficiencies for luminous giants.

To investigate whether or not the conclusions of Yan & Mateo (1994) are supported by the expanded sample of clusters in Table 4a, we have “predicted” binary fractions for the various radial velocity surveys using the Yan & Mateo (1994) short-period binary fraction and assuming: (1) a period distribution which is flat in  $\log P$ ; and (2) a period distribution identical to that observed by Duquennoy & Mayor (1991) for nearby solar-type stars (i.e., equation 4). The respective estimates,  $x'_b(\text{flat})$  and  $x'_b(\text{DM91})$ , are recorded in the fifth and sixth columns of Table 4a. For M71, the measured binary fraction agrees within its uncertainty with both the flat and DM91 distributions. In other words, M71 appears to be relatively abundant in *both* short- and long-period binaries. Similarly, both the flat and DM91 extrapolations are consistent with the measured binary fraction in M4 (which is a similar dynamical environment to M71). On the other hand, both extrapolations overpredict  $x_b$  for M22 and  $\omega$  Cen, clusters which have surveys sensitive to longer periods and considerably higher binary ionization rates (see below). Indeed, for these clusters,  $x_b$  and  $x'_b(\text{DM91})$  differ by nearly an order of magnitude. We conclude that, based on the expanded sample of clusters in Table 4a, the overabundance of short-period, eclipsing binaries compared to red-giant binaries noted by Yan & Mateo (1994) may, in fact, be stronger evidence for the disruption of dynamically-soft binaries rather than for a universal period distribution which is flat in  $\log P$ .

Is there evidence for the disruption of soft binaries in the radial velocity surveys alone? Table 4b records the clusters which have been searched for spectroscopic binaries, the binary fraction per decade of period, the logarithmic mean period of the survey, the one-dimensional velocity dispersion calculated with the maximum-likelihood estimator of Pryor & Meylan (1993) *and measured at the same radius as those stars monitored for velocity variability*,<sup>5</sup> the critical binary separation  $a_c$  estimated from equation 1, and the corresponding critical binary period  $P_c$  for a pair of  $0.8M_\odot$  stars. In Figure 8 we show the binary fraction per decade of period plotted against: (1) the logarithmic mean period of each survey; (2) the critical binary separation; (3) the critical binary period; and (4) the ratio of the critical binary period to the logarithmic mean period of the survey. Although the uncertainties in the measured binary fractions remain rather large,

---

<sup>5</sup>For the clusters reviewed in Hut et al. (1992), we give the mean  $\sigma_{1D}$ , weighted by the number of stars in each cluster.

these figures demonstrate that M22 and  $\omega$  Cen — clusters which have the largest  $P_{\max}$  and the smallest  $P_c$  — have the lowest binary fractions. Similarly, those clusters with the largest  $P_c/\langle P \rangle$  (e.g., M71, M4 and NGC 3201) have the highest binary fractions in the sample. It is, of course, possible that *external* processes have modified the binary fraction in a few of these clusters (for instance, the large number of binaries in M71 might be due, in part, to the enhancement of the binary fraction by tidal stripping; McMillan & Hut 1994). It should also be kept in mind that the above estimates of  $a_c$  and  $P_c$  do not include *all* of the environmental factors governing binary destruction: for example, the center of  $\omega$  Cen does not appear to satisfy equation 2, nor does this equation take into account the shrinking of hard binaries with wide orbits via energy exchanges with passing stars (see equation 2 of Phinney 1996). Nevertheless, these values should be a reasonable first approximation to the amount of binary destruction expected. We therefore conclude that both the number of short-period eclipsing binaries relative to long-period radial velocity variables *and* the radial velocity surveys alone point to a frequency-period distribution in which binaries with periods in excess of the “hard-soft transition” have been disrupted by stellar encounters (Heggie 1975; Hills 1984). *To the best of our knowledge, this is the first observational evidence for the destruction of soft binaries in globular clusters.*

Finally, we note that three stars which have previously been identified as members of the rare breed of globular cluster CH stars are included in our sample: III-106 (Hesser, Hartwick & McClure 1977; McClure & Norris 1977), IV-24 (Hesser & Harris 1979) and III-78 (Lloyd Evans 1978). Continued monitoring of the radial velocities of field CH stars has conclusively demonstrated (McClure & Woodsworth 1990) that many, perhaps even all, of these systems are binaries. Although the number of velocities for each CH star in our survey is small (III-106 – three measurements; IV-24 and III-78 – two measurements each), the combined chi-squared for these three objects is 5.04 for four degrees of freedom, which corresponds to  $P(\chi^2) = 0.28$ . Therefore, there is, at present, no evidence that any of the CH stars in M22 are members of binary systems. A similar result has recently been reported by Mayor et al. (1996), who found only two binaries among 32 chemically peculiar (Ba, CH and S) stars in  $\omega$  Cen. Such a result can be understood if these stars are simply otherwise normal outliers in the cluster metallicity distribution function or if they were enriched via mass exchange with companions which have subsequently been disrupted. However, the field CH stars studied by McClure & Woodsworth (1990) have periods near 3 years, whereas such systems would be dynamically hard in M22. According to Hills (1984), binaries with periods less than  $\simeq 25$  years are expected to have escaped disruption, for an assumed one-dimensional velocity dispersion of  $6.6 \text{ km s}^{-1}$  (Peterson & Cudworth 1994). Available evidence therefore suggests that the carbon enhancement seen in

the M22 CH stars is probably *not* the result of mass transfer. Indeed, Vanture & Wallerstein (1992) have recently carried out an abundance analysis of III-106 and have argued that it is not a genuine CH star in the sense applied to field CH stars. Rather, it appears to be an otherwise normal giant whose carbon excess has arisen from incomplete CN processing relative to other M22 giants.

We thank Roger Griffin and Jim Gunn for providing the crucial first epoch of radial velocities. We also extend our thanks to the staff and night assistants of all three observatories for their fine support. We are especially grateful to Tom Ingerson and Nick Suntzeff for donating a portion of an Argus engineering night which was used to obtain some of the radial velocities presented in this paper. The research of CP on binary stars in globular clusters was supported by NSF Grant AST-9020685.

## REFERENCES

- Anthony-Twarog, B. J., Twarog, B. A., & Craig, J. 1995, *PASP*, 107, 32
- Arp, H. C., & Melbourne, W. G. 1959, *AJ*, 64, 28
- Alcaino, G., Liller W., & Alvarado F. 1988, *ApJ*, 330, 569
- Barden, S. C., Armandroff, T. E., & Pryor, C. 1996, in *The Origins, Evolution and Destinies of Binary Stars in Clusters*, edited by E. F. Milone, in press
- Cohn, H. 1980, *ApJ*, 242, 765
- Côté, P., Welch, D.L., Fischer, P., Da Costa, G. S., Tamblyn, P., Seitzer, P., & Irwin, M. J. 1994, *ApJS*, 90, 83
- Côté, P., Welch, D. L., Fischer, P., & Gebhardt, K. 1995, *ApJ*, 454, 788
- Côté, P., & Fischer, P. 1996, *AJ*, submitted
- Côté, P., Fischer, P., Gebhardt, K., Williams, T.B, Pryor, C. 1996, in preparation
- Cudworth, K. M. 1986, *AJ*, 92, 348
- Djorgovski, S. G. & King, I. R. 1986, *ApJ*, 305, L61
- Djorgovski, S. G. 1993, in *The Structure and Dynamics of Globular Clusters*, ASP Conference Series, Vol 50, edited by S. G. Djorgovski and G. Meylan, (ASP, San Francisco), p. 373
- Duquennoy, A., & Mayor, M. 1991, *A&A*, 248, 485
- Fletcher, J. M., Harris, H. C., McClure, R. D., & Scarfe, C. D. 1982, *PASP*, 94, 1017
- Gebhardt, K., Pryor, C., Williams, T. B., & Hesser, J. E. 1995, *AJ*, 110, 1699
- Griffin, R. F., & Gunn, J. E. 1974, *ApJ*, 191, 545
- Gunn, J. E., & Griffin, R. F. 1979, *AJ*, 84, 752
- Hesser, J. E., & Harris, G. L. H. 1979, *ApJ*, 234, 513



- Hesser, J. E., Hartwick, F. D. A., McClure, R. D. 1977, *ApJS*, 33, 471
- Hills, J. G. 1984, *AJ*, 89, 1811
- Heggie, D. C. 1975, *MNRAS*, 173, 729
- Heggie, D. C. 1980, in *Globular Clusters*, NATO Adv. Study Institute, ed. D. Hanes & B. Madore (Cambridge Univ. Press), p. 281
- Hoffer, J. B. 1983, *AJ*, 88, 1420
- Hut, P., & Bahcall, J. N. 1983, *ApJ*, 268, 319
- Hut, P., McMillan, S., Goodman, J., Mateo, M., Phinney, E. S., Pryor, C. P., Richer, H. B., Verbunt, F., & Weinberg, M. 1992, *PASP*, 104, 981
- Lloyd Evans, T. 1975, *MNRAS*, 171, 647
- Lloyd Evans, T. 1978, *MNRAS*, 182, 293
- Lupton, R. H., Gunn, J. E., & Griffin, R. F. 1987, *AJ*, 93, 1114
- Mateo, M. 1993, in *Blue Stragglers*, ed. R. Saffer, (San Francisco: ASP), p. 74
- Mateo, M. 1996, in *The Origins, Evolution and Destinies of Binary Stars in Clusters*, edited by E. F. Milone, in press
- Mayor, M., Benz, W., Imbert, M., Martin, N., Prevot, L., Andersen, J., Nordström, B., Ardeberg, A., Lindgren, H., & Maurice, E. 1984, *A&A*, 134, 118
- Mayor, M., Duquennoy, A., Udry, S., Andersen, J., & Nordström, B. 1996, in *The Origins, Evolution and Destinies of Binary Stars in Clusters*, edited by E. F. Milone, in press
- McClure, R. D., & Norris, J. 1977, *ApJ*, 216, L101
- McClure, R. D., & Woodsworth 1990, *ApJ*, 352, 709
- McMillan, S., & Hut, P. 1994, *ApJ*, 427, 793
- Peterson, R. C., & Cudworth, K. M. 1994, *ApJ*, 420, 612

- Peterson, R. C., Rees, R. F., & Cudworth, K. M. 1995, *ApJ*, 443, 124
- Phinney, E. S. 1996, in *The Origins, Evolution and Destinies of Binary Stars in Clusters*, edited by E. F. Milone, in press
- Pryor, C., Latham, D. W., & Hazen, M. L. 1988, *AJ*, 96, 123
- Pryor, C., McClure, R. D., Fletcher, J. M., & Hesser, J. E. 1989, *AJ*, 98, 596
- Pryor, C., Fletcher, J. M., Hesser, J. E., McClure, R. D., Stetson, P. B., Richer, H. B., Fahlman, G. G., Ibata, R. A., Ivanans, N. C., Mandushev, G., Bell, R. A., Bolte, M., Bond, H. B., Harris, W. E., VandenBerg, D. A., & Wood, M. A. 1996, In *Dynamical Evolution of Star Clusters – Confrontation of Theory and Observations*”, IAU Symp 174, eds J. Makino & P. Hut, in press.
- Pryor, C., & Meylan, G. 1993, in *The Structure and Dynamics of Globular Clusters*, edited by S.G. Djorgovski & G. Meylan, (ASP, San Francisco), p. 357
- Sawyer-Hogg, H. 1973, *Publ. David Dunlap Obs.*, 3, 6.
- Shawl, S. J., and White, R. E. 1986, *AJ*, 91, 312
- Sigurdsson, S., & Phinney, E. S. 1993, *ApJ*, 415, 631
- Stetson, P. B., Davis, L. E., & Crabtree, D. R. 1990, in *CCDs in Astronomy*, ASP Conference Series, Vol.25, edited by G. H. Jacoby (ASP, San Francisco), p. 297
- Stetson, P. B. 1994, *PASP*, 106, 250
- Trager, S., King, I. R., & Djorgovski, S. G. 1995, *AJ*, 109, 218
- Vanture, A. D., & Wallerstein, G. 1992, *PASP*, 104, 888
- Yan, L., & Mateo, M. 1994, *AJ*, 108, 1810
- Zinn, R., & Searle, L. 1976, *ApJ*, 209, 734

Table 1. Log of Spectroscopic Observations

Date m/y	Telescope	Instruments	$N_{V_r}$	$N_*$
05/1972	Hale 5-m	Palomar RVS	19	18
06/1974	Hale 5-m	Palomar RVS	31	31
05/1975	Hale 5-m	Palomar RVS	17	17
06/1985	SAO 1.5-m	echelle + Reticon	10	10
07/1986	MMT 4.5-m	echelle + Reticon	122	94
11/1986	MMT 4.5-m	echelle + Reticon	4	2
05/1987	MMT 4.5-m	echelle + Reticon	39	33
07/1989	CFHT 3.6-m	DAO RVS	36	36
05/1991	CFHT 3.6-m	DAO RVS	13	11
06/1994	CTIO 4.0-m	Argus + echelle	92	92

Table 2. Radial Velocities for M22 Giants

Star	ID	R '	$\theta$ deg	HJD -2440000.0	$v_r$ km s <sup>-1</sup>	$\bar{v}_r$ km s <sup>-1</sup>	$\chi^2$	P( $\chi^2$ )	V mag	B-V mag	Source
1	V8 <sup>a</sup>	1.5	212.9	1460.970	-146.67±0.64	-147.21±0.32	6.48	0.000	10.83	1.92	P
				2199.970	-148.69±0.69						P
				2557.920	-149.74±0.67						P
				6636.659	-141.63±0.99						S
				6923.997	-149.16±1.11						S
				9511.908	-143.87±1.01						T
2	V5 <sup>a</sup>	3.2	255.8	2199.960	-157.55±0.73	-156.54±0.42	0.64	0.587	10.86	1.55	P
				2557.970	-156.81±0.84						P
				6636.660	-155.89±0.90						S
				9511.908	-155.36±0.90						T
3	IV-202	7.4	170.7	2199.980	-152.24±0.88	-152.24±0.88			11.04	1.74	P
4	IV-97	5.6	137.3	1461.990	-151.06±0.78	-150.24±0.46	8.68	0.000	11.07	1.76	P
				6636.650	-152.75±0.75						S
				9511.924	-145.85±0.87						T
5	IV-102	6.1	153.7	1461.990	-140.34±0.70	-140.71±0.31	2.45	0.032	11.08	1.72	P
				2199.990	-137.27±0.83						P
				2557.930	-140.62±0.79						P
				6636.670	-142.29±0.75						S
				7717.937	-140.81±0.78						C
				9511.916	-142.58±0.80						T
6	C	6.3	330.7	2199.930	-154.32±0.75	-154.32±0.75			11.10	1.87	P
7	III-208	12.0	196.7	2199.990	-146.06±0.71	-146.06±0.71			11.11	1.86	P
8	V9 <sup>a</sup>	3.8	257.3	2199.960	-148.79±0.76	-146.31±0.40	7.75	0.000	11.13	2.11	P
				2557.970	-142.29±0.74						P
				6636.670	-145.35±0.85						S
				9511.924	-149.40±0.84						T
9	III-3	1.5	261.4	1460.990	-150.20±0.65	-148.26±0.30	0.87	0.515	11.16	1.80	P
				2199.940	-148.57±0.91						P
				2557.990	-147.27±0.71						P
				6923.990	-147.46±0.88						S
				7717.939	-147.38±0.75						C
				8404.057	-147.50±0.95						C
				9511.924	-148.55±0.77						T
10	III-14	2.2	251.5	1460.980	-152.06±0.66	-150.98±0.36	1.97	0.096	11.19	1.83	P
				2557.890	-148.27±0.78						P
				6923.990	-152.72±0.97						S
				7717.941	-151.19±0.85						C
				8404.065	-150.84±0.91						C
11	V-9	0.3	188.6	2199.950	-144.45±0.70	-143.49±0.47	3.71	0.024	11.34	1.78	P
				7718.004	-140.57±0.88						C

Table 2 cont'd. Radial Velocities for M22 Giants

Star	ID	R '	$\theta$ deg	HJD -2440000.0	$v_r$ km s <sup>-1</sup>	$\overline{v}_r$ km s <sup>-1</sup>	$\chi^2$	P( $\chi^2$ )	V mag	B-V mag	Source
				8404.111	-144.96±0.90						C
12	III-26	1.8	199.7	1460.970	-147.47±0.75	-146.52±0.54	1.41	0.236	11.35	1.77	P
				2199.970	-145.49±0.78						P
13	III-15	2.1	247.6	1460.980	-147.74±0.68	-147.47±0.37	1.43	0.222	11.36	1.65	P
				2199.970	-148.49±0.95						P
				6924.000	-144.45±1.14						S
				7717.943	-146.96±0.77						C
				9511.908	-148.33±0.76						T
14	V-5	0.7	194.8	2199.940	-163.64±0.91	-163.73±0.46	1.16	0.325	11.38	1.73	P
				2557.940	-161.48±1.13						P
				7717.998	-164.97±0.82						C
				8404.075	-163.75±0.86						C
15	II-26	2.7	306.3	2199.910	-131.47±1.35	-131.24±0.73	0.03	0.870	11.39	1.71	P
				2557.960	-131.14±0.86						P
16	II-97	1.3	278.9	1460.990	-138.63±0.90	-138.63±0.90			11.42	1.60	P
17	I-202	1.2	48.4	1461.980	-152.60±0.77	-151.85±0.51			11.42	1.64	P
				2199.870	-151.24±0.69						P
18	IV-17	1.4	163.8	1460.960	-158.42±0.82	-158.09±0.52	0.11	0.739	11.44	1.76	P
				2199.950	-157.87±0.68						P
19	II-67	1.4	305.1	1460.990	-152.85±1.01	-152.85±1.01			11.44	1.81	P
20	V-2	1.2	135.2	1460.960	-141.08±0.76	-140.90±0.34	0.36	0.834	11.46	1.67	P
				2199.950	-140.09±0.83						P
				7717.996	-141.94±0.73						C
				8404.070	-140.78±0.82						C
				8405.067	-140.41±0.72						C
21	V-23	1.1	43.3	1461.000	-138.25±1.01	-140.78±0.36	18.8	0.000	11.47	1.56	P
				2199.860	-139.91±0.62						P
				7718.017	-150.76±0.90						C
				8404.126	-137.91±0.90						C
				8405.070	-138.19±0.80						C
22	IV-204	11.0	174.8	2199.990	-150.49±1.03	-150.49±1.03			11.50	1.63	P
23	III-52	3.2	267.4	2199.920	-151.43±0.78	-151.95±0.40	1.35	0.256	11.51	1.67	P
				6919.900	-150.40±0.90						S
				7717.949	-151.50±0.87						C
				9511.916	-153.68±0.72						T
24	V-12	0.9	236.6	2199.940	-144.43±1.00	-144.71±0.54	1.53	0.217	11.53	1.54	P
				7718.006	-146.28±0.88						C
				8404.116	-143.13±0.95						C
25	III-112	2.0	216.1	2199.980	-158.27±0.90	-158.27±0.90			11.53	1.54	P
26	II-80	1.3	0.8	1461.980	-136.19±0.79	-136.53±0.55	0.15	0.695	11.54	1.71	P

Table 2 cont'd. Radial Velocities for M22 Giants

Star	ID	R '	$\theta$ deg	HJD -2440000.0	$v_r$ km s <sup>-1</sup>	$\bar{v}_r$ km s <sup>-1</sup>	$\chi^2$	P( $\chi^2$ )	V mag	B-V mag	Source
				2199.960	-136.85±0.77						P
27	I-121	1.5	81.9	2199.870	-142.87±0.83	-142.87±0.83			11.55	1.44	P
28	III-12	2.3	262.3	1460.980	-149.92±0.82	-150.18±0.35	0.67	0.610	11.56	1.64	P
				6219.894	-149.00±1.00						S
				6636.660	-149.95±0.69						S
				7717.945	-149.81±0.74						C
				9511.931	-151.72±0.75						T
29	I-92	2.7	51.7	1461.980	-156.57±0.92	-155.69±0.40	0.21	0.890	11.57	1.55	P
				6219.930	-155.30±0.70						S
				7717.947	-155.47±0.77						C
				9511.939	-155.76±0.83						T
30	II-96	1.6	270.7	1460.990	-164.86±1.95	-162.91±0.38	0.73	0.601	11.59	1.48	P
				1461.960	-163.23±0.86						P
				2557.950	-161.73±0.96						P
				6219.900	-162.20±0.90						S
				7717.952	-164.26±0.80						C
				9511.908	-162.18±0.89						T
31	I-112	3.2	48.9	2558.880	-142.25±0.94	-142.25±0.94			11.65	1.49	P
32	I-12	2.9	15.0	2199.910	-143.61±0.85	-142.43±0.41	0.65	0.582	11.69	1.45	P
				6219.920	-143.00±0.90						S
				7717.954	-141.78±0.78						C
				9511.908	-141.65±0.78						T
33	II-99	2.7	343.7	2199.930	-142.75±0.95	-142.75±0.95			11.70	1.49	P
34	II-205	0.4	303.8	2557.950	-162.59±0.99	-162.59±0.99			11.86	1.45	P
35	II-101	4.1	312.7	2199.930	-157.33±0.80	-157.33±0.80			11.88	1.57	P
36	IV-205	0.8	147.2	2557.930	-158.49±1.20	-158.49±1.20			11.92	1.38	P
37	V-22	0.9	33.9	1461.970	-147.67±0.92	-146.73±0.47	0.52	0.592	11.92	1.47	P
				7718.015	-146.74±0.76						C
				8405.072	-146.00±0.81						C
38	II-31	3.5	292.4	2199.920	-156.12±0.94	-156.74±0.40	1.37	0.241	11.93	1.49	P
				6219.916	-155.40±0.80						S
				6636.650	-158.14±0.91						S
				7717.956	-156.44±0.79						C
				9511.931	-158.80±1.13						T
39	I-36	1.5	67.2	2199.880	-140.55±1.00	-140.47±0.49	0.53	0.662	11.94	1.32	P
				6219.940	-139.20±1.00						S
				7717.959	-141.31±0.83						C
				9511.939	-140.44±1.19						T
40	III-111	1.5	258.1	2557.940	-142.56±0.98	-142.56±0.98			11.98	1.42	P
41	I-37	1.4	74.9	2199.870	-158.51±0.97	-158.38±0.40	0.58	0.626	11.99	1.35	P

Table 2 cont'd. Radial Velocities for M22 Giants

Star	ID	R '	$\theta$ deg	HJD -2440000.0	$v_r$ km s <sup>-1</sup>	$\bar{v}_r$ km s <sup>-1</sup>	$\chi^2$	P( $\chi^2$ )	V mag	B-V mag	Source
42	I-8	3.4	19.1	6219.940	-157.30±0.80	-153.20±0.49	1.79	0.147	12.00	1.41	S
				7717.958	-158.22±0.83						C
				9511.950	-159.25±0.70						T
				2199.900	-150.72±1.00						P
				6636.670	-154.38±0.80						S
				7717.963	-153.53±0.91						C
43	I-57	3.4	73.3	9511.931	-153.75±1.46	-161.87±0.47	0.35	0.702	12.01	1.49	T
				6636.670	-162.32±0.74						S
				7717.961	-161.84±0.72						C
44	II-1	1.5	358.0	9511.924	-160.90±1.13	-165.08±0.55	0.08	0.783	12.08	1.52	T
				2199.890	-165.25±0.72						P
				2557.960	-164.84±0.84						P
45	IV-20	1.8	167.4	6219.876	-166.30±0.70	-166.82±0.19	0.40	0.989	12.09	1.48	S
				6635.820	-167.23±0.94						S
				6635.847	-167.49±0.88						S
				6636.647	-167.13±0.71						S
				6636.662	-167.36±0.80						S
				6636.684	-165.99±0.78						S
				6636.781	-165.79±0.88						S
				6637.794	-167.19±0.75						S
				6742.559	-166.67±0.79						S
				6743.553	-165.62±0.92						S
				6744.549	-166.80±1.02						S
				6923.957	-166.21±0.87						S
				6923.982	-167.41±1.04						S
				6924.951	-167.14±0.79						S
				6924.990	-167.05±0.81						S
				6927.899	-167.63±0.93						S
				6927.937	-166.28±0.69						S
				7717.965	-167.16±0.86						C
				9511.931	-168.77±1.28						T
46	III-96	5.7	242.6	6636.680	-141.70±0.92	-141.74±0.55	0.17	0.842	12.11	1.34	S
				7717.970	-142.12±0.85						C
				9511.916	-141.11±1.14						T
47	II-30	3.4	299.0	6636.650	-149.22±1.12	-148.59±0.62	0.42	0.656	12.19	1.38	S
				7717.972	-148.00±0.83						C
				9511.924	-149.56±1.63						T
48	C697	6.2	341.4	6636.680	-144.07±0.84	-144.10±0.55	0.64	0.528	12.21	1.29	S
				7717.968	-143.31±0.96						C
				9511.939	-145.29±1.14						T

Table 2 cont'd. Radial Velocities for M22 Giants

Star	ID	R '	$\theta$ deg	HJD -2440000.0	$v_r$ km s <sup>-1</sup>	$\bar{v}_r$ km s <sup>-1</sup>	$\chi^2$	P( $\chi^2$ )	V mag	B-V mag	Source
49	V-8	0.6	129.1	7718.002	-144.13±0.86	-144.64±0.63	0.48	0.488	12.22	1.28	C
				8405.083	-145.21±0.91						C
50	IV-88	4.8	99.4	6633.911	-144.10±0.80	-144.80±0.45	1.41	0.239	12.23	1.38	S
				6635.843	-145.91±0.93						S
				7717.974	-143.72±0.82						C
				9511.924	-146.47±1.09						T
51	III-106 <sup>b</sup>	5.1	223.7	6635.840	-155.60±0.85	-155.14±0.45	1.03	0.357	12.23	1.45	S
				7717.976	-153.91±0.80						C
				9511.931	-155.78±0.70						T
52	III-33	2.7	200.3	6223.920	-146.30±0.70	-146.83±0.26	0.81	0.625	12.24	1.32	S
				6635.751	-147.08±1.00						S
				6635.797	-146.34±1.01						S
				6635.818	-145.12±0.85						S
				6635.846	-146.72±1.22						S
				6636.669	-146.85±0.94						S
				6636.717	-146.76±0.86						S
				6636.812	-147.15±0.75						S
				6637.785	-147.62±0.94						S
				6637.828	-145.91±1.02						S
				7717.978	-147.65±0.85						C
				9511.931	-149.47±1.13						T
53	V-18	0.6	63.6	7718.009	-143.25±0.91	-141.71±0.68	4.52	0.033	12.28	1.35	C
				8405.074	-139.78±1.02						C
54	V-19	0.4	13.8	7718.011	-142.66±0.88	-142.36±0.65	0.17	0.680	12.29	1.34	C
				8405.077	-142.01±0.96						C
55	IV-76	2.6	100.7	6639.770	-150.42±1.05	-151.05±0.55	0.73	0.482	12.30	1.32	S
				7717.984	-150.76±0.78						C
				9511.916	-152.42±1.14						T
56	II-98	3.2	300.8	6636.680	-149.78±0.86	-149.05±0.58	0.64	0.526	12.31	1.38	S
				7717.986	-148.76±0.94						C
				9511.916	-147.69±1.45						T
57	I-86	3.2	34.4	6223.929	-140.60±0.90	-139.73±0.48	0.47	0.706	12.31	1.39	S
				6639.761	-139.82±1.02						S
				7717.980	-138.84±0.83						C
				9511.924	-139.93±1.19						T
58	II-104	5.0	311.3	6635.840	-136.79±1.06	-136.07±0.62	2.50	0.082	12.32	1.40	S
				7717.988	-136.50±0.85						C
				9511.931	-132.02±1.81						T
59	I-98	2.4	11.4	6639.780	-135.58±1.32	-135.46±0.53	0.01	0.990	12.33	1.25	S
				7717.990	-135.51±0.79						C



Table 2 cont'd. Radial Velocities for M22 Giants

Star	ID	R '	$\theta$ deg	HJD -2440000.0	$v_r$ km s <sup>-1</sup>	$\bar{v}_r$ km s <sup>-1</sup>	$\chi^2$	P( $\chi^2$ )	V mag	B-V mag	Source
60	III-47	2.4	244.0	9511.950	-135.35±0.85	-142.47±0.60	1.42	0.242	12.37	1.26	T
				2557.900	-141.63±0.89						P
				6639.800	-144.23±1.09						S
				9511.924	-141.84±1.21						T
61	I-27	2.0	46.6	2557.980	-129.57±1.14	-129.49±0.52	2.33	0.072	12.38	1.20	P
				6639.790	-127.51±1.00						S
				7717.992	-129.78±0.84						C
				9511.908	-132.59±1.43						T
62	III-35	2.4	201.2	2557.910	-158.49±1.27	-160.12±0.73	7.03	0.001	12.38	1.27	P
				6923.970	-158.33±1.12						S
				9511.939	-165.25±1.45						T
63	I-85	3.6	33.5	6639.770	-148.09±1.24	-147.68±1.06	0.35	0.555	12.41	1.22	S
				9511.916	-146.61±2.02						T
64	I-113	3.9	40.1	6635.840	-139.04±1.22	-141.40±0.96	8.34	0.004	12.41	1.34	S
				9511.908	-145.21±1.55						T
65	IV-67	2.5	118.7	6635.830	-156.90±1.09	-156.13±0.90	1.37	0.241	12.41	1.36	S
				9511.931	-154.42±1.62						T
66	V-4	1.0	171.8	6923.980	-149.62±1.57	-149.43±1.01	0.02	0.884	12.42	0.95	S
				9511.950	-149.30±1.31						T
67	3-9	6.0	319.6	6635.840	-146.13±1.08	-145.88±0.67	0.07	0.798	12.44	1.36	S
				9511.924	-145.72±0.86						T
68	III-86	3.8	226.1	6635.830	-153.66±1.06	-152.99±0.89	1.21	0.272	12.46	1.29	S
				9511.916	-151.32±1.67						T
69	I-106	2.0	63.0	6923.970	-153.33±1.05	-153.10±0.83	0.10	0.746	12.47	1.21	S
				9511.924	-152.72±1.35						T
70	IV-33	5.6	172.1	6635.830	-155.45±0.99	-156.20±0.90	2.91	0.088	12.49	1.26	S
				9511.908	-159.65±2.12						T
71	IV-100	6.5	135.6	6635.810	-151.97±1.09	-150.75±0.92	3.87	0.049	12.52	1.22	S
				9511.931	-147.68±1.73						T
72	I-68	4.8	61.5	6635.830	-143.31±1.06	-143.61±0.88	0.23	0.634	12.52	1.23	S
				9511.931	-144.29±1.59						T
73	C712	7.0	336.1	6635.820	-143.96±1.00	-143.67±0.78	0.17	0.680	12.52	1.31	S
				9511.939	-143.23±1.24						T
74	I-80	4.8	34.9	6635.820	-150.29±0.94	-151.16±0.79	2.47	0.116	12.54	1.35	S
				9511.939	-153.26±1.46						T
75	C175	2.0	94.8	6923.990	-151.72±1.22	-152.14±0.94	0.25	0.615	12.55	1.22	S
				9511.939	-152.76±1.49						T
76	IV-110	6.7	94.6	6635.820	-150.26±1.02	-150.14±0.81	0.03	0.858	12.55	1.36	S
				9511.924	-149.93±1.34						T
77	III-39	3.2	207.7	6635.810	-151.44±0.94	-151.11±0.83	0.51	0.475	12.57	1.23	S

Table 2 cont'd. Radial Velocities for M22 Giants

Star	ID	R '	$\theta$ deg	HJD -2440000.0	$v_r$ km s <sup>-1</sup>	$\bar{v}_r$ km s <sup>-1</sup>	$\chi^2$	P( $\chi^2$ )	V mag	B-V mag	Source
				9511.908	-149.90±1.80						T
78	IV-31	3.7	171.9	6635.810	-152.81±0.99	-152.81±0.99			12.58	1.27	S
79	2-6	4.6	293.0	6635.810	-150.79±1.14	-151.04±0.89	0.10	0.746	12.58	1.40	S
				9511.924	-151.43±1.44						T
80	II-23	2.6	320.0	6927.930	-143.11±0.86	-143.81±0.77	2.99	0.084	12.63	1.26	S
				9511.931	-146.66±1.73						T
81	IV-24 <sup>b</sup>	2.2	162.8	6924.990	-159.60±0.84	-160.05±0.78	1.90	0.168	12.64	1.32	S
				9511.924	-162.84±2.09						T
82	I-53	3.2	87.2	6927.920	-145.54±1.09	-145.25±0.98	0.35	0.553	12.69	1.28	S
				9511.939	-143.98±2.30						T
83	I-58	3.6	77.8	6635.760	-144.44±1.36	-141.65±1.02	8.69	0.003	12.71	0.96	S
				9511.908	-138.07±1.54						T
84	V-7	1.1	147.5	6924.980	-152.36±0.86	-152.69±0.75	0.55	0.459	12.73	1.32	S
				9511.939	-153.75±1.54						T
85	I-51	2.8	86.8	6924.980	-152.24±0.99	-152.11±0.79	0.04	0.834	12.77	1.21	S
				9511.950	-151.87±1.32						T
86	II-42	3.5	271.1	6635.800	-150.09±0.97	-150.21±0.91	0.13	0.721	12.78	1.24	S
				9511.908	-151.12±2.65						T
87	III-93	5.8	250.8	6635.665	-143.42±1.01	-144.26±0.27	0.99	0.457	12.79	1.19	S
				6635.704	-143.72±0.98						S
				6635.739	-143.38±1.12						S
				6635.759	-141.96±1.14						S
				6635.792	-143.34±1.11						S
				6635.831	-146.94±1.19						S
				6636.677	-144.29±0.83						S
				6636.759	-144.33±1.11						S
				6636.809	-144.49±0.97						S
				6637.744	-144.20±1.17						S
				6637.819	-144.60±0.87						S
				6638.761	-143.89±0.97						S
				6639.752	-145.92±1.28						S
				6927.913	-144.90±1.08						S
				9511.939	-146.95±1.92						T
88	I-11	2.9	11.8	6927.920	-146.65±1.01	-145.95±0.92	2.52	0.112	12.79	1.32	S
				9511.939	-142.73±2.17						T
89	I-110	1.7	15.9	6924.980	-148.15±1.11	-147.91±0.99	0.22	0.643	12.80	1.27	S
				9511.924	-146.96±2.23						T
90	II-9	3.7	349.6	6635.810	-150.46±0.90	-149.85±0.78	1.63	0.201	12.80	1.28	S
				9511.916	-148.04±1.55						T
91	II-102	4.9	357.2	6635.800	-137.98±0.95	-137.96±0.90	0.00	0.953	12.81	1.20	S

Table 2 cont'd. Radial Velocities for M22 Giants

Star	ID	R '	$\theta$ deg	HJD -2440000.0	$v_r$ km s <sup>-1</sup>	$\bar{v}_r$ km s <sup>-1</sup>	$\chi^2$	P( $\chi^2$ )	V mag	B-V mag	Source
92	I-54	2.8	72.5	9511.931	-137.81±2.68	-155.55±0.83	5.76	0.016	12.81	1.25	T
				6927.910	-156.31±0.89						S
				9511.916	-149.98±2.41						T
93	IV-101	5.8	147.3	6635.790	-145.75±1.28	-145.75±1.28			12.82	1.10	S
94	I-116	4.0	78.5	6635.790	-155.48±1.15	-155.04±1.05	0.84	0.359	12.82	1.10	S
				9511.916	-152.82±2.59						T
95	III-6	1.5	236.9	6924.980	-158.23±1.04	-158.14±0.84	0.02	0.890	12.82	1.26	S
				9511.950	-157.97±1.44						T
96	III-17	2.0	240.3	6927.920	-153.53±1.09	-153.87±0.93	0.32	0.571	12.85	1.29	S
				9511.916	-154.75±1.76						T
97	III-45	2.3	229.3	6927.920	-148.02±0.94	-148.02±0.94			12.86	1.23	S
98	IV-40	4.0	161.2	6635.660	-142.27±0.98	-142.27±0.98			12.88	1.18	S
99	V-17	1.0	91.3	6927.910	-149.54±1.08	-150.10±0.99	1.70	0.193	12.88	1.18	S
				9511.931	-153.21±2.54						T
100	3-270	6.3	10.6	6635.790	-148.15±0.95	-147.90±0.85	0.33	0.563	12.90	1.24	S
				9511.939	-146.87±1.92						T
101	II-100	3.6	323.5	6635.660	-141.56±1.01	-141.02±0.95	2.57	0.109	12.99	1.17	S
				9511.939	-136.57±2.90						T
102	III-78 <sup>b</sup>	4.5	205.6	6635.670	-152.99±0.94	-153.34±0.88	1.08	0.298	12.99	1.24	S
				9511.924	-155.80±2.48						T
103	IV-96	5.8	133.5	6635.670	-153.87±1.28	-154.32±0.98	0.27	0.600	13.04	1.15	S
				9511.950	-154.94±1.51						T
104	III-46	2.4	239.8	6924.960	-156.91±1.15	-157.80±0.78	0.99	0.372	13.04	1.19	S
				6927.934	-158.10±1.17						S
				9511.939	-160.87±2.60						T
105	IV-3	1.4	111.5	6927.900	-140.32±1.09	-140.15±1.00	0.16	0.692	13.04	1.21	S
				9511.924	-139.22±2.51						T
106	II-44	2.7	276.0	6927.900	-145.29±1.01	-145.29±1.01			13.05	1.19	S
107	III-79	4.8	210.6	6635.680	-148.83±1.05	-148.58±1.00	0.61	0.433	13.06	1.18	S
				9511.931	-146.06±3.34						T
108	III-75	4.3	199.3	6635.680	-147.74±1.09	-147.74±1.09			13.10	1.05	S
109	III-87	3.9	232.8	6635.710	-159.45±0.99	-159.45±0.99			13.10	1.28	S
110	II-105	5.6	298.6	6635.700	-141.56±1.05	-142.04±0.89	0.69	0.405	13.10	1.33	S
				9511.950	-143.24±1.66						T
111	II-106	5.9	289.8	6635.700	-148.86±1.14	-149.22±1.06	0.71	0.400	13.11	1.14	S
				9511.939	-151.45±2.82						T
112	III-115	3.7	206.1	6635.680	-138.38±1.26	-138.38±1.26			13.14	1.11	S
113	C319	6.7	135.6	6924.960	-151.13±1.15	-151.37±1.04	0.24	0.621	13.14	1.12	S
				9511.908	-152.49±2.46						T
114	III-19	2.0	230.3	6927.900	-149.04±1.06	-148.71±0.97	0.57	0.449	13.14	1.18	S

Table 2 cont'd. Radial Velocities for M22 Giants

Star	ID	R '	$\theta$ deg	HJD -2440000.0	$v_r$ km s <sup>-1</sup>	$\bar{v}_r$ km s <sup>-1</sup>	$\chi^2$	P( $\chi^2$ )	V mag	B-V mag	Source
115	C684	6.6	354.9	9511.950	-147.01±2.42						T
				6635.710	-148.25±1.15	-148.12±1.06	0.09	0.770	13.14	1.20	S
				9511.916	-147.36±2.78						T
116	IV-66	2.8	123.5	6927.930	-150.12±0.92	-150.19±0.89	0.07	0.785	13.17	1.17	S
				9511.916	-151.08±3.37						T
117	I-107	2.4	67.5	6924.950	-149.52±1.02	-149.10±0.94	1.11	0.292	13.18	1.16	S
				9511.950	-146.72±2.42						T
118	I-115	4.5	54.6	6635.770	-143.90±1.17	-144.95±1.05	4.03	0.045	13.19	1.09	S
				9511.908	-149.31±2.39						T
119	I-117	4.3	89.8	6635.690	-152.18±1.04	-152.53±0.94	0.56	0.453	13.19	1.20	S
				9511.931	-154.00±2.15						T
120	I-118	6.2	40.0	6635.690	-141.48±1.11	-141.48±1.11			13.20	1.21	S
121	IV-104	6.2	178.7	6635.780	-147.94±1.38	-147.94±1.38			13.24	1.07	S
122	IV-99	6.6	132.8	6635.780	-155.99±0.90	-156.17±0.84	0.32	0.572	13.24	1.16	S
				9511.916	-157.45±2.39						T
123	3-171	5.9	17.3	6635.770	-135.86±1.04	-135.80±0.95	0.02	0.883	13.24	1.29	S
				9511.931	-135.47±2.41						T
124	3-190	6.1	338.5	6635.760	-152.78±1.24	-152.82±1.12	0.01	0.935	13.25	1.09	S
				9511.908	-153.02±2.63						T
125	III-117	5.7	189.9	6635.780	-151.31±0.98	-151.31±0.98			13.26	1.14	S
126	3-177	5.9	11.8	6635.770	-145.58±1.19	-145.21±1.04	0.41	0.522	13.26	1.21	S
				9511.916	-143.97±2.18						T
127	C635	1.6	318.0	6924.960	-146.79±1.08	-146.79±1.08			13.29	1.18	S
128	II-10	3.3	340.3	6635.750	-150.28±1.26	-150.28±1.26			13.33	1.17	S
129	IV-49	3.4	152.9	6635.750	-153.41±0.93	-153.41±0.93			13.36	1.06	S
130	III-51	2.8	256.0	6924.970	-144.11±1.17	-143.55±1.12	2.66	0.103	13.41	1.03	S
				9511.946	-137.58±3.82						T
131	IV-85	5.7	96.4	6635.740	-151.62±1.01	-151.52±0.87	0.04	0.840	13.42	1.16	S
				9511.950	-151.21±1.74						T
132	III-56	3.2	245.9	6635.730	-144.03±1.38	-144.03±1.23	0.00	0.995	13.48	1.19	S
				9511.931	-144.01±2.70						T
133	3-42	5.6	266.6	6635.730	-150.69±1.32	-150.69±1.32			13.51	1.14	S
134	3-112	5.4	141.3	6636.700	-144.72±1.17	-144.72±1.17			13.52	0.95	S
135	2-42	5.0	92.4	6636.690	-149.04±1.26	-149.04±1.26			13.52	0.97	S
136	3-88	5.8	187.1	6636.690	-155.39±1.12	-155.39±1.12			13.52	1.05	S
137	3-126	5.2	112.6	6635.720	-145.66±1.05	-145.62±1.02	0.03	0.855	13.53	1.14	S
				9511.908	-144.83±4.41						T
138	II-12	2.8	331.2	6924.970	-134.85±1.19	-133.95±1.09	3.43	0.064	13.53	1.23	S
				9511.916	-129.42±2.67						T
139	III-85	4.1	215.6	6637.801	-160.08±0.87	-160.26±0.62	0.08	0.775	13.56	1.16	S

Table 2 cont'd. Radial Velocities for M22 Giants

Star	ID	R '	$\theta$ deg	HJD -2440000.0	$v_r$ km s <sup>-1</sup>	$\bar{v}_r$ km s <sup>-1</sup>	$\chi^2$	P( $\chi^2$ )	V mag	B-V mag	Source
				6637.822	-160.44±0.88						S
140	I-61	3.5	67.1	6637.810	-155.96±1.26	-155.96±1.26			13.57	1.13	S
141	III-53	3.6	257.3	6637.810	-159.27±0.99	-159.27±0.99			13.58	1.17	S
142	III-10	1.7	252.5	6742.570	-150.97±1.41	-150.97±1.41			13.59	1.08	S
143	3-119	6.3	119.1	6636.740	-144.67±1.30	-144.67±1.30			13.60	1.04	S
144	IV-39	3.7	167.2	6637.790	-147.65±0.98	-147.65±0.98			13.61	1.07	S
145	III-82	3.7	211.0	6636.720	-155.85±0.86	-155.90±0.84	0.09	0.763	13.65	1.13	S
				9511.924	-157.24±4.52						T
146	2-73	4.6	0.5	6637.800	-127.65±1.12	-127.27±1.07	1.26	0.262	13.65	1.15	S
				9511.939	-123.48±3.54						T
147	I-73	3.8	53.4	6636.710	-141.21±1.22	-141.21±1.22			13.67	1.11	S
148	C507	6.7	240.1	6636.730	-153.04±1.22	-153.04±1.22			13.73	1.11	S
149	I-82	4.2	39.6	6636.740	-151.14±0.88	-151.14±0.88			13.76	1.13	S
150	C313	6.6	149.8	6636.760	-145.92±1.06	-145.92±1.06			13.79	1.04	S
151	3-8	6.2	319.0	6636.750	-137.92±1.12	-137.92±1.12			13.80	1.20	S
152	III-69	4.3	184.4	6636.770	-153.80±1.22	-153.80±1.22			13.81	1.07	S
153	2-33	4.4	142.6	6636.790	-142.45±1.02	-142.45±1.02			13.87	1.02	S
154	2-75	4.7	357.0	6636.780	-143.73±1.12	-143.73±1.12			13.88	1.13	S
155	2-69	4.5	12.6	6636.800	-152.14±1.17	-152.14±1.17			13.88	1.13	S
156	3-186	6.2	355.6	6637.750	-140.21±0.88	-140.21±0.88			13.91	1.13	S
157	IV-82	3.7	97.5	6637.760	-160.63±1.09	-160.63±1.09			13.92	1.06	S
158	C531	6.4	270.8	6637.780	-153.08±0.94	-153.08±0.94			13.92	1.16	S
159	I-63	3.8	67.3	6637.770	-149.49±0.87	-149.49±0.87			13.97	1.10	S

<sup>a</sup> Photometric variable according to Sawyer-Hogg (1973). Mean magnitudes and colors are from Peterson & Cudworth (1994).

<sup>b</sup> CH-enhanced star. See text for details.

Table 3. Dependence of Derived M22 Binary Fraction on Adopted Model Parameters

Model	$f(e)$	$P_{\min}$ (yr)	$P_{\max}$ (yr)	$f(P)$	$M_{2,\min}$ ( $M_{\odot}$ )	$M_{2,\max}$ ( $M_{\odot}$ )	$f(M_2/M_1)$	$\sigma_j^a$ ( $\text{km s}^{-1}$ )	$x_b$ Case A	Case B
a	Circular	0.1	40	DM91 <sup>b</sup>	0.08	0.8	DM91 <sup>c</sup>	0.9	0.00–0.01 (0.11) <sup>d</sup>	0.02–0.05 (0.18)
	Thermal	0.3	40	DM91	0.08	0.8	DM91	0.9	0.00–0.03 (0.19)	0.04–0.12 (0.29)
b	Circular	0.1	40	DM91	0.16	0.8	DM91	0.9	0.00–0.02 (0.10)	0.03–0.06 (0.16)
	Thermal	0.3	40	DM91	0.16	0.8	DM91	0.9	0.00–0.04 (0.16)	0.05–0.10 (0.25)
c	Circular	0.1	40	DM91	0.08	1.2	DM91	0.9	0.00–0.02 (0.11)	0.03–0.07 (0.17)
	Thermal	0.3	40	DM91	0.08	1.2	DM91	0.9	0.00–0.03 (0.17)	0.04–0.10 (0.30)
d	Circular	0.1	40	Flat	0.08	0.8	Flat	0.9	0.00–0.02 (0.11)	0.03–0.06 (0.19)
	Thermal	0.3	40	Flat	0.08	0.8	Flat	0.9	0.00–0.04 (0.20)	0.05–0.12 (0.34)
e	Circular	0.1	40	DM91	0.08	0.8	DM91	0.0	0.00–0.02 (0.12)	0.03–0.05 (0.19)
	Thermal	0.3	40	DM91	0.08	0.8	DM91	0.0	0.00–0.04 (0.19)	0.05–0.11 (0.29)
f	Circular	0.1	20	DM91	0.08	0.8	DM91	0.9	0.00–0.02 (0.10)	0.03–0.05 (0.15)
	Thermal	0.3	20	DM91	0.08	0.8	DM91	0.9	0.00–0.04 (0.16)	0.05–0.10 (0.27)
g	Circular	0.1	40	DM91	0.8	0.8	—	0.9	0.00–0.01 (0.06)	0.02–0.04 (0.09)
	Thermal	0.3	40	DM91	0.8	0.8	—	0.9	0.00–0.03 (0.13)	0.04–0.08 (0.19)

<sup>a</sup> Assumed amplitude of the velocity jitter at the tip of the red giant branch (see equation 2 in text).

<sup>b</sup>  $dN/d\log P \propto \exp(-\frac{(\log P - \overline{\log P})^2}{2\sigma_{\log P}^2})$  where  $P$  is in days,  $\overline{\log P} = 4.8$  and  $\sigma_{\log P} = 2.3$  (Duquennoy & Mayor 1991 = DM91)

<sup>c</sup>  $dN/dq \propto \exp(-\frac{(q - \overline{q})^2}{2\sigma_q^2})$  where  $\overline{q} = 0.23$  and  $\sigma_q = 0.42$  (Duquennoy & Mayor 1991)

<sup>d</sup> quantities in parentheses give the 90% confidence upper limits on the binary fraction (i.e.,  $x_b$  for which 5% of simulations give  $N_8$ ; lower limit on  $x_b$  is zero for all models).

Table 4a. Radial Velocity Searches for Binary Stars in Globular Clusters

Cluster(s)	$x_b$ <sup>a</sup>	Period Range	$x_b/\log(P_{\max}/P_{\min})$	$x_b'$ (flat)	$x_b'$ (DM91)
M22 <sup>b</sup>	0.01 (Cir)	$0.1^y - 40^y$	0.009	0.11	0.43
	0.03 (Thr)	$0.3^y - 40^y$		0.09	0.38
$\omega$ Cen <sup>c</sup>	0.035	$0.5^y - 25^y$	0.021	0.07	0.31
47 Tuc, M2, M3	0.07 (Cir)	$0.2^y - 20^y$	0.059	0.09	0.33
M71, M13, M12 <sup>d</sup>	0.17 (Thr)				
NGC 3201 <sup>e,f</sup>	$\leq 0.12$ (Cir)	$0.02^y - 15^y$	$\leq 0.062$	0.12	0.38
	$\leq 0.19$ (Thr)	$0.07^y - 15^y$		0.10	0.35
M71 <sup>g</sup>	0.20 (Cir)	$3^d - 10^y$	0.076	0.13	0.36
	0.27 (Thr)				
M4 <sup>h</sup>	0.20	$2^d - 3^y$	0.076	0.12	0.27

<sup>a</sup> Binary fraction for systems having mass ratios  $q \geq 0.1$ . Since the binary fractions quoted by Hut et al. (1992) and Côté & Fischer (1996) refer to binaries with  $q \gtrsim 0.2$ , we have multiplied their estimates by 1.39 (see Table 7 of Duquennoy & Mayor 1991).

Survey References: b – This Paper

c – Mayor et al. (1996)

d – Hut et al. (1992)

e – Côté et al. (1994)

f – Côté et al. (1996)

g – Barden et al. (1996)

h – Côté & Fischer (1996)

Table 4b. Radial Velocity Searches for Binary Stars in Globular Clusters

Cluster(s)	$x_b/\log(P_{\max}/P_{\min})$	$\langle \log P \rangle$ (P in year)	$\sigma_{1D}$ (km s <sup>-1</sup> )	$a_c$ (AU)	$P_c$ (year)	Reference <sup>a</sup>
M22	0.009	0.452	7.5	8.42	19.3	1
$\omega$ Cen	0.021	0.548	12.2	3.17	4.47	2
47 Tuc, M2, M3 M71, M13, M12	0.059	0.301	6.3	11.9	32.5	3
NGC 3201	$\leq 0.062$	-0.125	3.7	35.3	166	4
M71	0.076	-0.543	2.2	97.6	762	3
M4	0.076	-0.892	3.2	46.1	248	5

<sup>a</sup> References for velocity dispersions: (1) This Paper  
(2) Pryor & Meylan (1993)  
(3) Pryor et al. (1996), unpublished.  
(4) Côté et al. (1995)  
(5) Peterson, Rees & Cudworth (1995)



Fig. 1.— V-band finding chart for the six stars not included in previous photometric catalogs. The image measures  $13'.6 \times 11'.6$ .

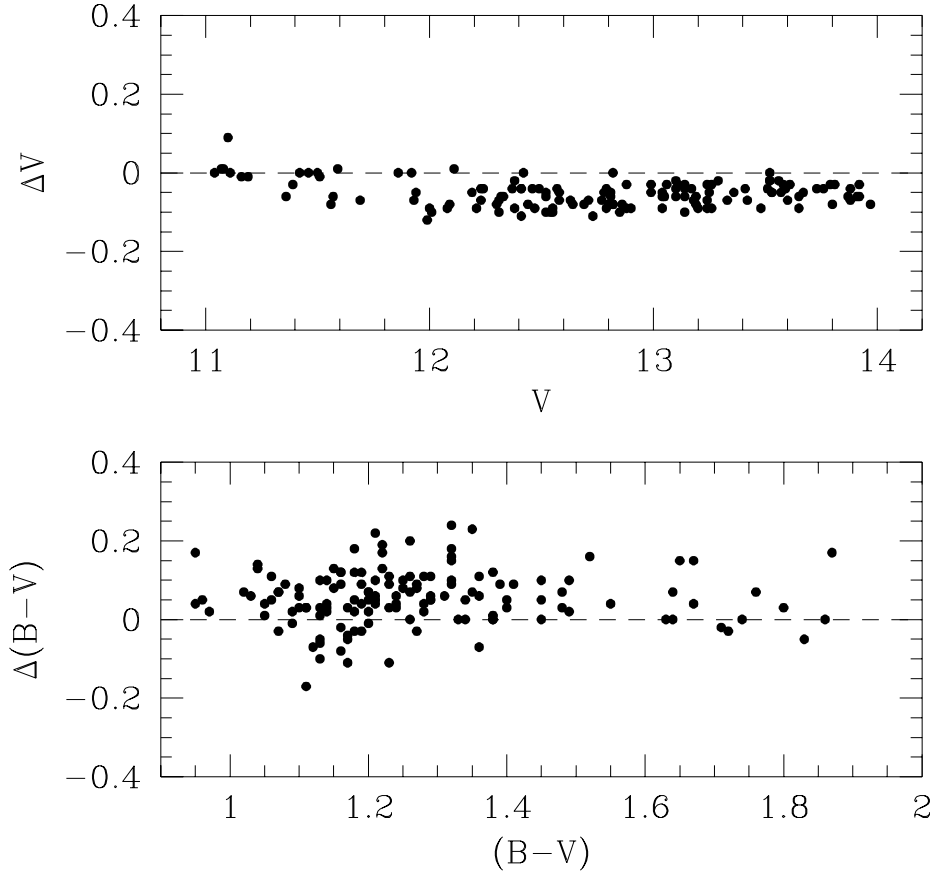


Fig. 2.— (Upper Panel) Relationship between the V magnitudes reported in this paper and the photographic values of Peterson & Cudworth (1994; PC) for the 137 stars in Table 2 which are common to both studies. The residuals are in the sense  $\Delta V = V_{\text{PC}} - V$ . (Lower Panel) Relationship between our (B-V) colors and those of Peterson & Cudworth (1994) for the same 137 stars. The residuals are in the sense  $\Delta(B-V) = (B-V)_{\text{PC}} - (B-V)$ .

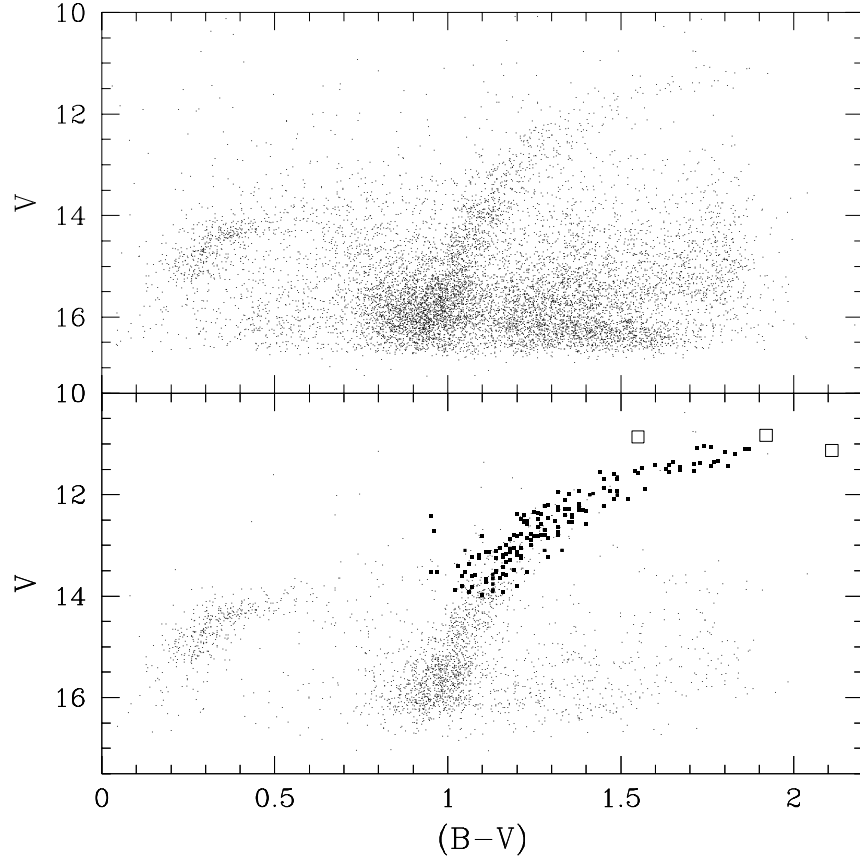


Fig. 3.— (Upper Panel) BV color-magnitude diagram for all 9752 stars contained within our  $43'.2 \times 43'.2$  field, based on data obtained with the KPNO 0.9m telescope and T2KA CCD. (Lower Panel) BV color-magnitude diagram for those 2539 stars within  $5r_c$  ( $r_c = 1'.42$  according to Trager, King & Djorgovski 1995) of the M22 cluster center (Shaw & White 1986). The stars for which we have multiple radial velocities are indicated by the filled squares. The large open squares show the three known photometric variables in our survey.

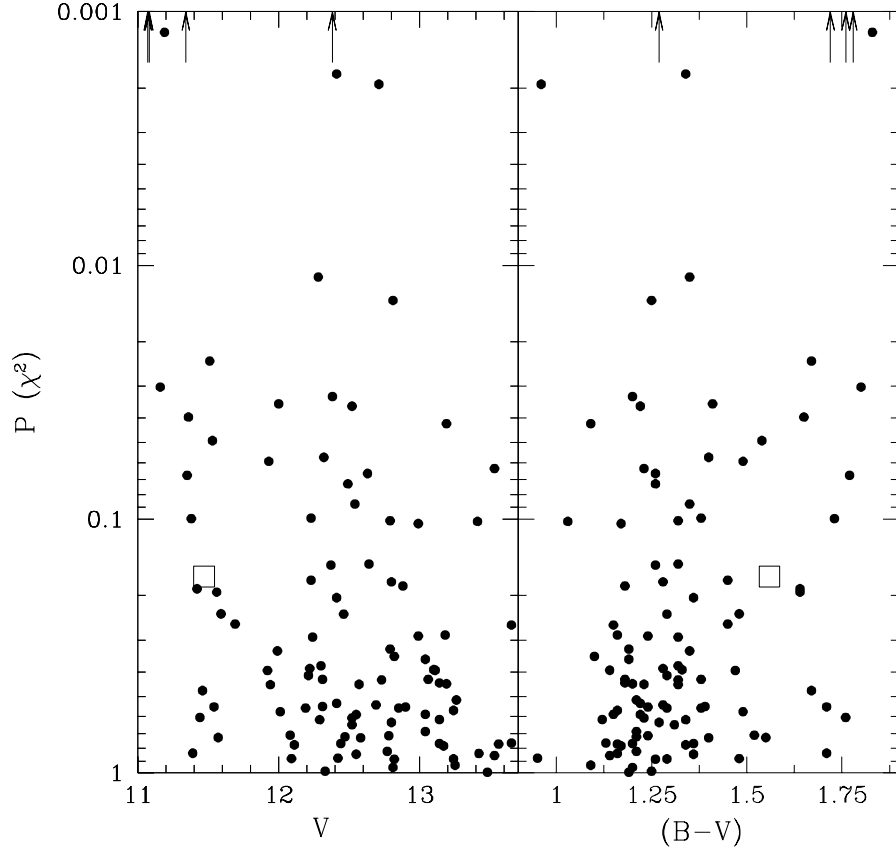


Fig. 4.— (Left Panel) Dependence of  $P(\chi^2)$  on  $V$  magnitude. No velocity jitter has been included in computing  $P(\chi^2)$ ;  $P(\chi^2) \approx 0$  otherwise. The four stars which have probabilities less than 0.001 are indicated by the vertical arrows. For V-23 (indicated by the open square), we have discarded the July 1989 CFHT velocity in computing  $P(\chi^2)$ ;  $P(\chi^2) \approx 0$  otherwise. (Right Panel) Dependence of  $P(\chi^2)$  on  $B-V$  color. Those stars with the lowest  $P(\chi^2)$  tend to lie near the tip of the red giant branch, consistent with previous findings (e.g., Mayor et al. 1984; Pryor, Latham & Hazen 1988) that the magnitude of the velocity jitter is a function of luminosity in these evolved stars.

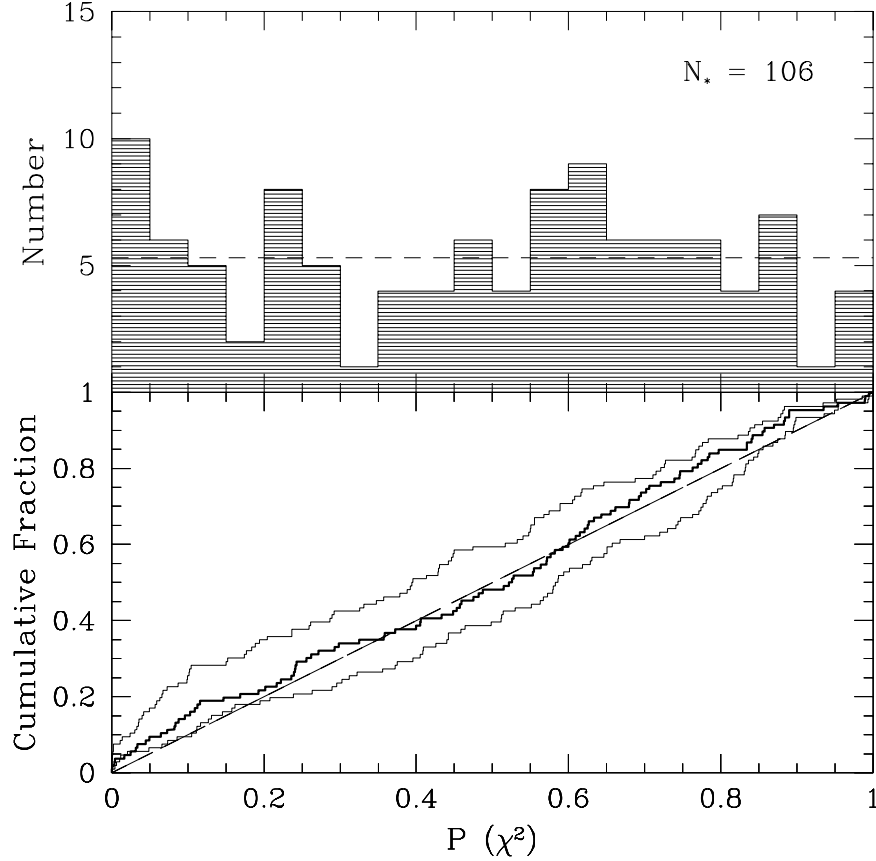


Fig. 5.— (Upper Panel) Distribution of  $P(\chi^2)$  for the 106 M22 red giants (i.e., three known photometric variables excluded) having multiple radial velocity measurements. We have assumed a velocity jitter of the form given by equation 3. The radial velocity measured for star V-23 in July 1989 has been omitted since it is likely to be a misidentification. A sample of constant-velocity stars is expected to show a flat distribution (dashed line), whereas that for a sample of radial velocity variables should be strongly peaked at  $P(\chi^2) \simeq 0$ . Apart from a modest peak near zero probability, the observed distribution is consistent with that expected for a population of constant-velocity stars. (Lower Panel) Cumulative distribution of  $P(\chi^2)$  for the same sample of M22 giants (heavy line). The upper and lower lines give the corresponding distributions assuming no jitter and a luminosity-independent jitter amplitude of  $1.5 \text{ km s}^{-1}$ , respectively. The dashed diagonal line shows distribution expected for a sample of constant-velocity stars.

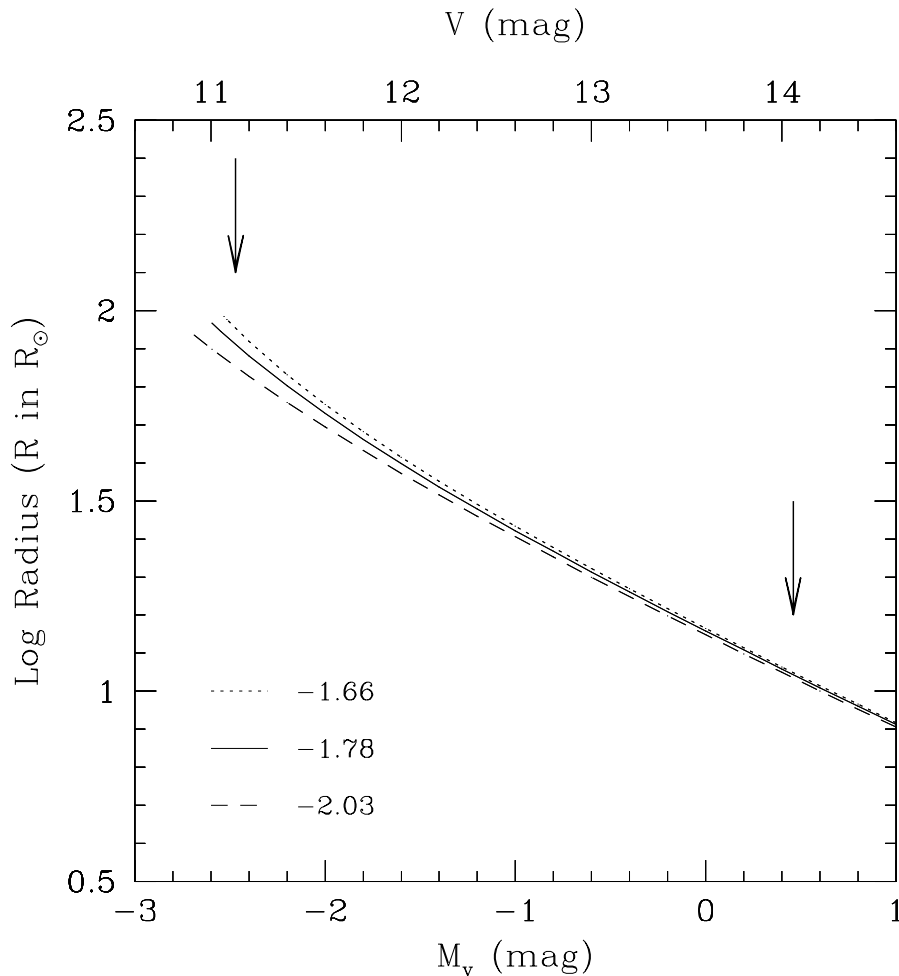


Fig. 6.— Relationship between stellar radius, V magnitude (upper axis) and absolute magnitude  $M_V$  (lower axis) for M22 red giants according to the 14 Gyr isochrones of Bergbusch & Vandenberg (1992). The three different curves have  $[\text{Fe}/\text{H}] = -2.03$ ,  $-1.78$  and  $-1.66$ , showing the dependence of radius on metallicity. The vertical arrows depict the magnitude limits of the survey, which correspond to maximum and minimum radii of  $\simeq 80$  and  $10R_\odot$ , respectively. In deriving the radii, we have interpolated in V using the  $[\text{Fe}/\text{H}] = -1.78$  isochrone and assumed  $(m-M)_V = 14.2$ ,  $M_V(\text{HB}) = 0.6$ ,  $E(B-V) = 0.37$  and  $A_V = 3.2E(B-V)$ .

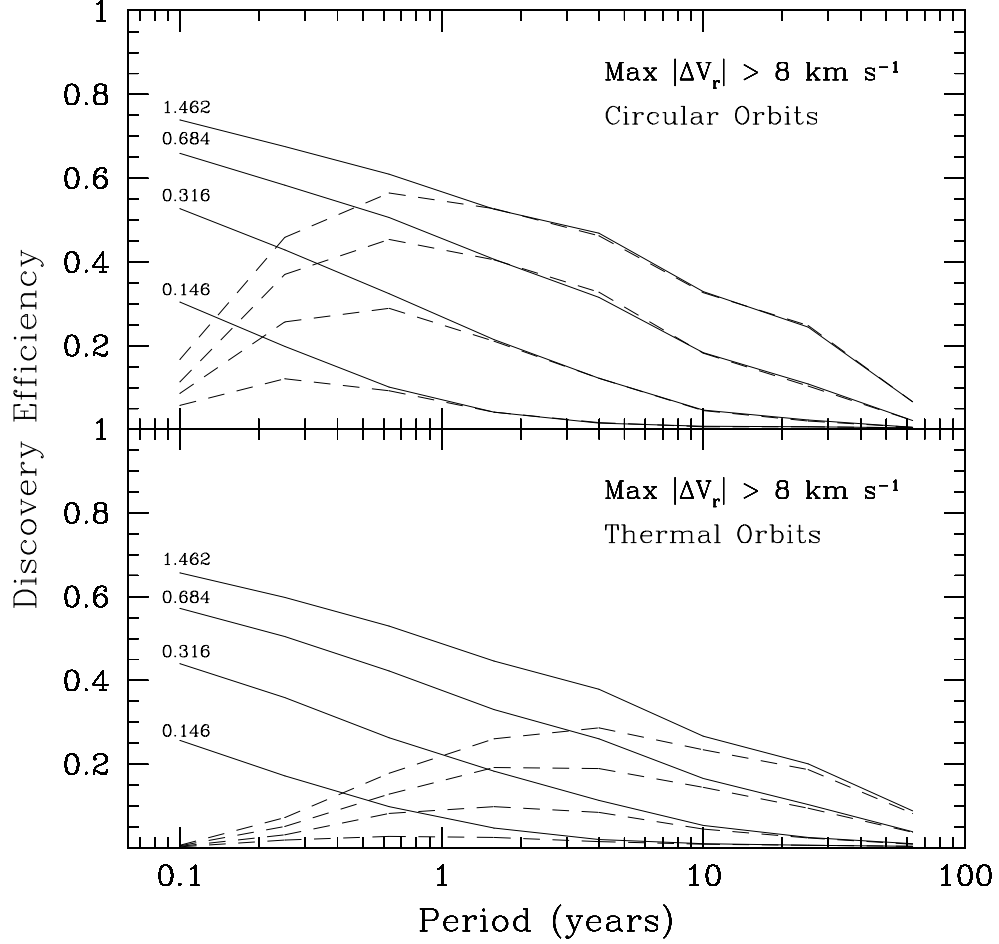


Fig. 7.— (Upper Panel) Binary discovery efficiencies based on the data given in Table 2 for the case of circular orbits. “Discovered” binaries are those which show a velocity variation larger than  $8 \text{ km s}^{-1}$ . From top to bottom, the four solid lines (labeled by the mean mass ratio in each bin) indicate the discovery efficiencies for systems having mass ratios in the intervals: (1)  $0.00 \leq \log q < 0.33$ ; (2)  $-0.33 \leq \log q < 0.00$ ; (3)  $-0.67 \leq \log q < -0.33$ ; and (4)  $-1.00 \leq \log q < -0.67$ . The dashed lines show the discovery efficiencies after taking into account selection effects caused by possible mass transfer between the binary components. (Lower Panel) Same as above, except for a thermal distribution of eccentricities.

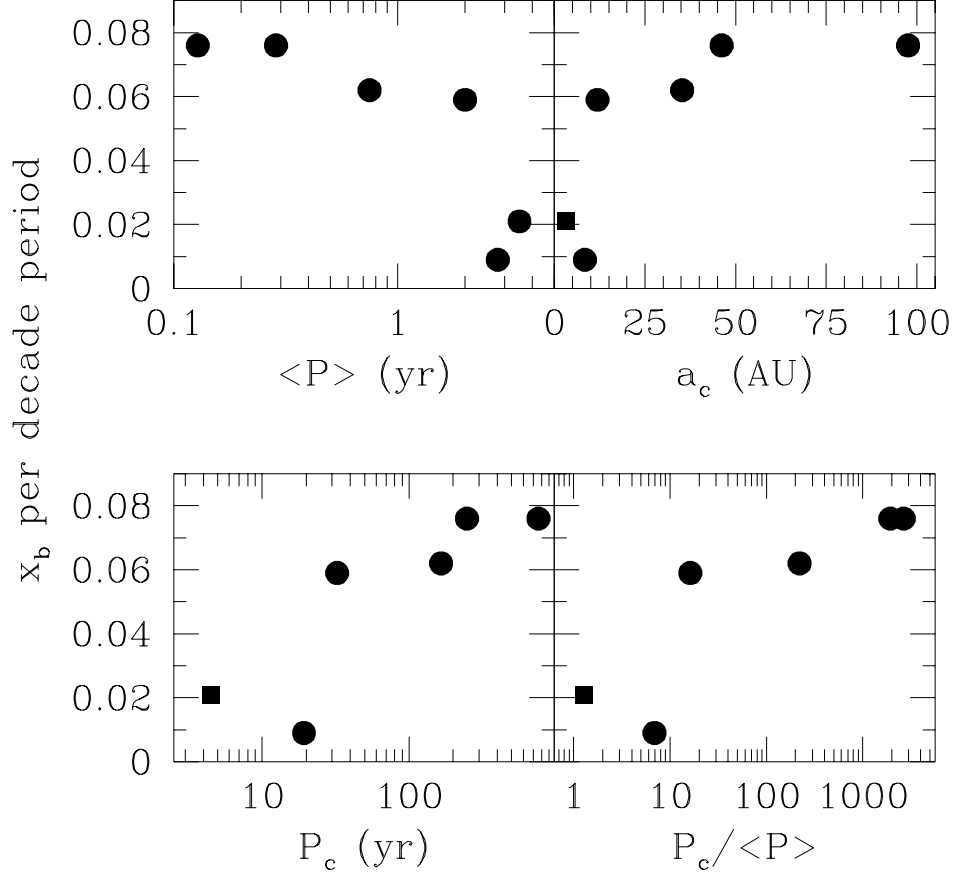


Fig. 8.— (Upper Left Panel) Binary fraction per decade of period plotted against the logarithmic mean period  $\langle P \rangle$  of each survey (see Table 4b). The binary fraction for NGC 3201 is probably best viewed as an upper limit (Côté et al. 1994; 1996). (Upper Right Panel) Binary fraction per decade of period plotted against the critical binary separation  $a_c$  computed with equation 1 (assuming  $M_1 = M_2 = 0.8M_\odot$ ). Note that  $\omega$  Cen, which is indicated by the closed square, does not satisfy equation 2. (Lower Left Panel) Binary fraction per decade of period plotted against the critical binary period  $P_c$  for a binary consisting of a pair of  $0.8M_\odot$  stars. (Lower Right Panel) Binary fraction per decade of period plotted against  $P_c / \langle P \rangle$ .